

UCSF

UC San Francisco Electronic Theses and Dissertations

Title

Pathogenic tau perturbs axonogenesis via loss of tau function

Permalink

<https://escholarship.org/uc/item/2bq8p1mx>

Author

Mohl, Gregory

Publication Date

2023

Peer reviewed|Thesis/dissertation

Pathogenic tau perturbs axonogenesis via loss of tau function

by
Greg Mohl

DISSERTATION
Submitted in partial satisfaction of the requirements for degree of
DOCTOR OF PHILOSOPHY

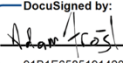
in

Biochemistry and Molecular Biology

in the

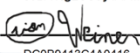
GRADUATE DIVISION
of the
UNIVERSITY OF CALIFORNIA, SAN FRANCISCO

Approved:

DocuSigned by:

91B1E6585191420... Adam Frost
Chair

DocuSigned by:

Martin Kampmann

DocuSigned by:

DC0B9413C4A0416... Orion Weiner

Committee Members

Dedication and Acknowledgements

I never would have been able to complete my PhD without the patient support of my colleagues, friends, and family. Graduate school was challenging in many ways, but the help was always there when we needed it.

I cannot thank Martin enough. You had endless energy to meet with me or instantly respond to emails while also balancing the many demands of being a professor. I knew that you would be an incredible mentor when I first heard you give a lecture. Thank you for inspiring me. You make mentoring and building an inclusive environment a top priority while also doing cutting-edge science. It's a rare combination. I also just must thank you for being so patient and supportive with the challenges of raising a family during graduate school. You literally saved us, twice!

I want to thank Emily Nieman for being the best teammate someone could ask for. Emily, you have worked incredibly hard, learned a ton, and have always maintained a positive attitude. I love joking around with you and listening to your music in 382B. I also love that you are a part of the family and that the girls just adore you. Thank you for helping me get across the finish line with graduate school. I could not have done it without you.

Gary Dixon, you were indispensable to the project and really saved it. It has been so fun to get to work with you, bounce crazy ideas off you, and just see the project take off ever since we joined forces. I really love working with you, and I wish you tremendous success as you continue in your career. Let's keep collaborating in the future!

I'd like to thank the members of the lab that have taken the time to help and mentor me over the years. Avi Samelson, for being my incredible rotation mentor, teaching me the ropes, and being a great friend. You have also had an enormous impact on my scientific training. Nina Draeger, for being so kind to me and always willing to help. Xiaoyan Guo, for inspiring me to join the lab and being a great example of an intrepid scientist. Ruilin Tian, for helping me with Crop-seq and being an amazing example to me. Kun Leng and Biswa Ramani for helping me move for 8 hours despite being two of the busiest people I know. I also have to thank Kun and Noam Teyssier for helping me so much with Crop-seq analysis. Both of you had a lot of patience and took a lot of time to teach me your ways. Biswa, thanks for being a great mentor to me. I miss having you in Sandler. I want to thank Anthony "AJ" Abarientos for working with me after Ruilin left. I want to thank Emmy Delaney, Jennifer Langen and Addie Cady for being wonderful rotation students and giving me the opportunity to learn to be a better mentor. I want to thank Sarah "SK" Kaufman for teaching me so much about the brain and being so open with advice about life and science. And importantly for teaching us all about Fast and the Furious! I want to thank Olivia Teter for being my partner in crime for that crazy symposium we planned that one time and for being just the greatest friend. It's been awesome working with you. I want to thank Emmy Li for always being willing to help me and for just being the best bench neighbor anyone could ask for. I want to thank Amanda McQuade for being the coolest postdoc ever and for giving the bluntest advice. Also I'm so glad we are book fans! It's fun to nerd out in lab. I want to thank Steven Boggess for being a great example to me and helping me get through those dark days in the pandemic. Vaidehi Gandhi, thank you for being such a joy to work with. Everytime you come to 382B (A lovely place to be), you always light up the room. Nabeela Ariqat, thank you for also being so fun to work with. You always had a great attitude no matter what was going on. You are one of the toughest people I know. Gio

Aviles, thank you for being my first and longest Kampmann lab friend. It was so fun growing up in science with you. Parker Grosjean, thank you so much for being my go to image analysis/ML wizard and for always being willing/excited to jump in and help. Brandon, DeSousa, thank you for being my go to Mitochondria wizard and for helping me so much with that terrible assay that you are so good at (Seahorse). Gokul, I've always looked up to you so much, and I think your project is so cool. That's probably why I got excited about the postdoc that I'm doing! Thanks for being a great friend and example. It's been fun playing pickleball with you lately! I want to thank Steph See, Gita Rohanitazangi, Jason Hong, Brendan Rooney, Sydney Sattler, Merissa Chen, Lydia Lee, Poornima Ramkumar, Joanna Chou, Jannis Buecking, Julianne Jin, Lin Yanadar, Venus Hagan, Spencer Danner-Bocks, Vincent Cele Castillo, Vasileios Papakis, Kunal Shroff, Indigo Rose, and everyone else who has come through the Kampmann Lab while I was here for making it such a thrilling and delightful place to work.

I want to thank my collaborators who have helped move this project forward. Justin McKetney and Danielle Swaney, thank you for the essential proteomics experiments. Your data really helped us figure out the axonogenesis mechanism. I'd like to thank members of the Nakamura lab, including Joyce Yang, Jonathan Meng and Neal Bennett for collaborating with us to uncover differential regulation of metabolism. I'd also like to thank our Cryo-TEM collaborators Gong Her Wu, Wah Chiu, Leslie Thompson, and Charlie Smith-Geater. I'd like to thank our ribosome profiling collaborators Jin Young Kim, J. Wren Kim and Nick Ingolia. I want to thank Ian Steele and Stephanie Huard for working with me on the tauopathy mice and Carlo Condello for teaching me how to use his microscope and for letting me work with his students! I want to thank Maxence Le Vassieur and Jodi Nunnari for working on us with the mitochondria story. I want to thank

Garrett Greenan for taking the time to begin teaching me to Fib-SEM. I also must thank Kari Herrington and the Center for Advanced Light Microscopy for the many hours teaching me how to use all of the microscopes. We really had some fun times! And I need to finish that book with you!

I also want to thank the wonderful UCSF and Tetrad community that helped shape my scientific career. My rotation mentor David Agard was my first major mentor at UCSF and helped set the tone for inspiring and welcoming me. Plus it was a huge privilege to work directly with one of my scientific heroes right off the bat. I also want to thank my Qualls committee members Ken Nakamura and Stephen Floor for helping me conceptualize my project. I want to thank Wallace Marhsall and Jennifer Fung for teaching the incredible Cellular Robotics class. Joseph Bondy-Denomy, thank you for mentoring me for the Bioreg proposal. Maxence Nachury, thank you for helping me prepare my journal club presentation. Todd Nystul and Seemay Chou, thank you for helping to recruit me to UCSF (you really made me feel welcome!). Barbara Panning, Rushika Perera, Peter Walter, Shaeri Mukherjee, Kaveh Ashrafi, thank you so much for making the Tetrad community so warm and scientifically thrilling to be a part of. Tom Kornberg, thank you for giving me a ride up the hill to Aldea! David Morgan, thank you for being super welcoming when I came to UCSF. You were really kind and helped make me feel like I belonged here. Geeta Narlikar, thank you for taking time out of your schedule to meet with me about family logistics/crises. You really go above and beyond for the students in your care. Toni Hurley, Danny Dam, and Billy Luh, thank you so much for helping me so frequently with program logistics and keeping Tetrad such a well-oiled machine.

I'd like to thank my committee members, Adam Frost and Orion Weiner. Adam, thank you for being such a wonderful example and mentor to me. You made me feel welcome when I first came to UCSF and in a big way inspired me to come train here. I learned about your work in my biochemistry class at BYU and we were all blown away by how cool it was! Thank you for helping me with my project by always questioning my assumptions. And, thank you for also meeting with me to discuss career development. You had a big impact on me.

Orion, thank you for being an incredible rotation mentor, friend, quals committee member, and thesis committee member. You have had an outsized impact on my scientific career. I love how you approach and think about science. The rotation was such a great experience from start to finish. It was really one of the toughest choices I've made to decide between joining your lab and Martin's. I hope we can keep in touch and to be able to give back to my communities in the future as you do.

I'd like to thank my rotation mentors for helping me get started at UCSF. Daniel Coutandin, you showed me what it means to work extremely hard. Thanks for teaching me! Brian Graziano, thank you for taking the time to really mentor me and help me stay excited about science. Avi, I can't thank you enough!

I'd also like to thank my biotech enthusiast community here at UCSF. It's been a privilege to be a part of both the Evexia Biofund and the Bay Area Nucleate Activator program.

I'd especially like to thank Matt Callahan for helping me get into Evexia and just being a great friend. It's been so fun to swap stories and to learn from you. I'd also like to thank the Evexia

leadership for putting so much time and energy into the community: Ian Steele, Paul Burroughs, Raymond Dai, Zach Gardell, Helen Sun and Chad Altobelli. I'd like to thank my ATP team, Neha Prasad, Cody Marhsall, and Christopher Teixeira, for working hard with me to try and find good investments. I also want to thank our coaches, Larry Zhu, Jinsoo Chung, and Paul Burroughs, for taking time to meet and mentor us. Greyson Lewis, thanks for mentoring me in my early Evexia days and for helping me expand my network. I will pay it forward!

I also want to thank the Bay Area Nucleate leadership team and the Ciznor team for the incredible opportunity to work with you over the past year. Nucleate has been really transformative for me and for my career. Zach Cogan, thank you for introducing me to Nucleate and supporting me through the ups and downs of starting a company. Andrew Pan, thanks for being a great friend and giving honest feedback about our prospects. Alina and Sasha, thanks for the many hours you put in to make Nucleate an awesome experience for everyone. I'd like to also thank Justin Olshavsky for really going above and beyond to give honest and open feedback about Ciznor that was critical for us. Kevin Holden, thanks for being a wonderful teammate and a great friend. I learned a lot from you. Tandin Vazin, thank you for teaching me so much about business. I'd also like to thank my friends at Avidity Life Sciences for taking a chance on me and supporting me. Avereigh Clarke, you have been with me on this journey for years! I always love talking science with you and I look forward to continuing to collaborate. Josh Flade and Alec Ferguson, thank you for being great friends and teaching me so much.

Claire Clelland, thanks for taking me on so early and allowing me to really see the process of starting a company from day 1. It has been a true privilege to be able to work with you, and I am so excited to see where this goes!

I wouldn't be here without the incredible mentors that I had during my undergraduate studies at BYU. Special thanks to David Busath, who took a chance on me and let me really have almost complete academic freedom to pursue my ideas. What a huge privilege that was! I'd also like to thank David Michaelis for taking a chance on me as well. It was so fun to work with you. I love your energy! Thanks for continuing to mentor me. Brad Berges, thank you for being a wonderful teacher, mentor, and member of my honor's thesis committee. Arminda Suli, thank you for teaching me so much during my time there and for working with me. It was a privilege!

I'd also like to thank the dear friends that we've made over the last few years here in San Francisco. This is a wonderful but sometimes challenging place to live. But with everyone's support, it has been really fun. Chris and Sabrina Vandiford, thank you so much for adopting our kids and just being so open with us. I love you guys! Sabrina, sorry Chris and I always geek out. Avereigh and Brianna Clarke, you really welcomed us to the city! We miss you dearly but are so happy that we get to see you relatively often when we go to Utah. Becca and Trevor Higginson, you will always have a special place in my heart. Thank you for watching Olivia in our dire time of need and for just being wonderful lifelong friends. Spencer and Sarah Vernon, thank you for helping us get through COVID and just being so lovely. We really miss you guys! I also really want to thank Ryan and Jaquel Jones, Max and Rachel Fillmore, Kinda and Jake Soujah, Allan and Brionne Carroll, Marc and Kelly Berbert, Sterling and Rachel DeMille, Bret and Rebekah Jackson, Rachel

Crane, Sophia Meurs, Chase and Jordan Wheeler, Lisa Poulson, Ammon and Mai Kaopua, and many, many others who have touched our lives so profoundly while living here in San Francisco.

I love and appreciate all of you!

I have enjoyed tremendous support from my family. Grandma Judy, I love you so much. Thanks for being a cheerleader and friend to me. Poppy, I love you and miss you already. I am motivated to work harder because of what you have had to endure. Grandpa Greg and CC, thank you for always believing in me and being so interested in my work! I love catching up with you and miss getting to see you more. Thanks for coming to visit us! Mema, I know you are proud of me! I miss you. Mepa, thank you for being a wonderful friend to me. I love you and am so excited to see you again. Grandma and Grandpa Lilya, thank you for your support and visits! Sandy and Ann Lilya, thanks for being such good friends to us.

I have many more people to thank! Brett and Jonny Overcash, thanks for being wonderful mentors and friends to me. Jenny and Kevin Moss, thank you for taking me in all those years ago and really helping me take off. Tyler and Shelby Moss, thanks for being such wonderful friends, my ping pong rival and guitar buddy respectively. Brad Yates, thanks for being a kind friend. Brooke and Cody Hyer, thanks for always being willing to let us drop in on them with barely a moment's notice. Amanda and Ed, thanks for going on outdoor adventures with us and being such good sounding boards. Tess, thanks for being a lifelong friend.

I also want to thank my new family, the Larsen crew. Your support, especially to Jaime through the ups and downs of graduate school, have been so vital. Alan Larsen thank you for the amazing

advice and endless support. Doneen, thank you for everything. But especially thank you for helping us survive having all these kids! Kari and Josh, thank you for loving and supporting us so much. Mark and Marissa, thank you for visiting us and being hilarious friends. Chelsie, thank you for being such a wonderful aunt and friend. Daryl and Rilla, thank you for being our comrades in graduate school/parent struggles. We love you guys! Chris, thanks for being the best uncle ever!

Mom and Dad, thank you so much for your support. I love you both very much, and I hope that you know that you have had a big influence on my life. I definitely would not be here without the countless hours you spent mentoring and teaching me over the years. More recently, thank you for visiting so frequently and being amazing grandparents! To my siblings, thank you for being the most fun group of trolls someone could ask for. I love you all so much!

I want to thank my kids for just being so wonderful. You guys really helped me stay focused on what really matters in life and not get sucked into lab too much. I have loved watching you grow up throughout graduate school!

Finally, I want to thank my wife Jaime. You have been so supportive and patient through all of the late nights, the massive stress of COVID, and the ups and downs of my project and career trajectory. I know how much you have sacrificed to help me become a scientist, and I will never forget it. I love you, and I'm excited for these next chapters of our lives!

Contributions

This dissertation was carried out under the guidance of Dr. Martin Kampmann, with feedback and collaboration from many members of the Kampmann lab. In particular, Gary Dixon contributed many datasets to this work and is going to be a co-first author on our peer-reviewed manuscript. Emily Nieman performed many of the experiments and analyses related to the axon branching phenotypes. My committee members Dr. Orion Weiner and Dr. Adam Frost also provided insightful feedback that helped guide this project. Other collaborators that contributed key data or reagents to this project include Justin McKetney, Danielle Swaney, Avi Samelson, and Judith Steen. At the time of dissertation submission, this work is pending publication. We are preparing a manuscript for submission pending additional ongoing *in vivo* experiments and a draft preprint will be published on BioRxiv.

Pathogenic tau perturbs axonogenesis via loss of tau function

Greg Mohl

Abstract

Neurodegenerative diseases are a major public health burden. There are only a few effective therapies because the underlying disease mechanisms are poorly understood. Tau aggregation is a hallmark of several neurodegenerative diseases, including Alzheimer's disease and frontotemporal dementia. There are causal disease variants of the tau-encoding gene, *MAPT*, and the presence of tau aggregates is highly correlated with disease progression. The molecular mechanisms linking pathological tau to neuronal dysfunction are not well understood. A major challenge for the tau field is a lack of clarity around tau's normal function in development and disease and how these processes change in the context of causal disease variants or amyloid beta plaques.

To address these questions in an unbiased manner, we conducted multi-omic characterization of iPSC-derived neurons harboring the *MAPT* V337M mutation, which revealed major changes in regulators of axonogenesis. *MAPT* V337M neurons have increased axon branching. Pathogenic tau mutations have generally been assumed to act through a gain of toxic function, leading to therapeutic approaches aiming to lower tau levels that are currently in clinical trials.

Surprisingly, we found that tau knockdown did not rescue axon branching in *MAPT* V337M neurons, and tau knockdown induced axon branching in *MAPT* WT neurons, strongly supporting a tau loss of function effect. Intriguingly, knockdown the tau-interacting protein *MYO1B* also increases axon branching in wild-type neurons without modifying axon branching in *MAPT* V337M neurons. We conclude that the FTD-associated tau mutation *MAPT* V337M drives major changes in neuronal differentiation and maturation caused by loss of tau function.

Table of Contents

CHAPTER 1: Pathogenic tau perturbs axonogenesis via loss of tau function.....	1
1.1 INTRODUCTION.....	1
1.2 RESULTS.....	3
1.3 DISCUSSION.....	27
1.4 MATERIALS AND METHODS.....	32
1.5 REFERENCES.....	43

List of Figures

Figure 1.1 RNA-seq in <i>MAPT</i> V337M neurons reveals conserved changes in axonogenesis that mirrors tau reduction in <i>MAPT</i> WT neurons.....	5
Figure 1.2 ATAC-seq uncovers tau dependent and independent regulators of gene expression in <i>MAPT</i> Het, <i>MAPT</i> WT and <i>MAPT</i> WT tau knockdown neurons.....	9
Figure 1.3 Proteomics shows convergence on altered regulation of axonogenesis protein levels and phosphorylation in neurons with <i>MAPT</i> V337M.....	12
Figure 1.4 <i>MAPT</i> V337M induces axon branching in differentiating neurons without substantially perturbing other parameters of neurite outgrowth.....	17
Figure 1.5 <i>MAPT</i> knockdown and <i>MYO1B</i> knockdown induce axon branching in <i>MAPT</i> WT neurons.....	19
Figure 1.6 <i>MAPT</i> V337M causes toxicity and hypersensitivity to mitochondrial stress...	21
Figure 1.7 <i>MAPT</i> V337M neurons have increased mitochondrial protein levels and Decreased mitophagy.....	23
Figure 1.8 <i>MAPT</i> V337M perturbs neurons via tau loss of function and tau gain of function.....	26

INTRODUCTION:

Neurodegenerative diseases are a growing public health burden and remain very challenging to treat because we lack a fundamental understanding of the underlying disease mechanisms. A common theme in many neurodegenerative diseases is the aggregation of pathological proteins, which was first described over one hundred years ago [1]. Tau aggregation is a hallmark of several neurodegenerative diseases, collectively called tauopathies, including Alzheimer's disease and Frontotemporal dementia. In Alzheimer's disease, tau aggregation and phosphorylation changes correlate better with disease progression than amyloid beta pathology [2] despite clear genetic evidence linking amyloid beta to the disease [3], leading to a more complex model where amyloid beta, pathological tau, immune activation, and synapse loss collaborate to drive disease. In Frontotemporal dementia, rare causal variants of tau that are fully penetrant for the disease give tau a more direct role in disease pathogenesis [4].

Despite the tremendous progress that has been made in the field, there are many unanswered questions about how pathogenic tau causes disease. Recent work has shown that pathogenic variants of tau sensitize neurons to many different types of cellular stress, and that this effect can be rescued by lowering tau levels via autophagy [5]. Other groups have shown that tau interferes with RNA splicing and stress granules homeostasis [6-9], disrupts the nuclear envelope [10-12], perturbs axonal trafficking [13, 14] or disrupts mitochondrial dynamics [15]. Acetylated tau has also been shown to disrupt chaperone mediated autophagy, rerouting tau and other clients to be degraded by other mechanisms [16]. Pathogenic tau has also been shown to perturb AIS plasticity and cause changes to neuronal excitability [17] and has been implicated in driving excitotoxicity [9, 18-20]. Many of these data support a tau toxic gain of function model, and tau

lowering has been successfully shown to be beneficial in cultured neurons and animal models [5, 21]. In fact, tau lowering is currently being tested in the clinic by antibodies and ASOs, and tau lowering is one of the most promising approaches for these devastating diseases [22]. It's clear from this broad body of work over the last 20 years that tau can induce many cellular phenotypes under different conditions and in different contexts.

We wanted to characterize the earliest potential changes that pathogenic tau causes in human neurons to understand mechanistically how pathogenic tau causes human disease. We also wanted to use a multi-omic approach to allow the data in an unbiased way to tell us which cellular phenotypes are most closely linked to pathogenic tau. This is essential because many focused studies have linked tau to diverse cellular processes that go awry in neurodegeneration but there are very few unbiased or comprehensive studies. We modeled pathogenic tau by using human iPSC derived neurons with the *MAPT* V337M mutation, a known cause of frontotemporal dementia.

We used two sets of induced pluripotent stem cells (iPSCs), one from a healthy donor (WTC11) and one from a patient with the *MAPT* V337M mutation (GIH6C1) [17, 23]. Our system has several advantages over mice, primary neurons, or human cancer cell lines. We can edit human cells from the same individual to generate isogenic pairs of cells with the same genetic background, including from patients that we know have or will develop the actual disease we are studying. We can generate homogenous cultures at scale with genetic and/or pharmacological perturbations to enable deep mechanistic characterization. A major limitation of prior work

studying pathogenic tau in cancer cell lines is that the key biology of tau that we and others have identified occurs in a neuron-specific context [REFs].

Our RNA-seq, ATAC-seq, proteomics and phosphoproteomics results all point directly to changes in axonogenesis due to the *MAPT* V337M mutation. We measured neurite outgrowth directly with longitudinal imaging and showed that *MAPT* V337M containing neurons as well as tau knockdown neurons have increased axon branching without changes to other aspects of neuron morphology. We show that loss of *MYO1B*, a top differential interactor of P301L and V337M variants of tau from previously published work [24], is sufficient to drive the changes in axon branching. We characterized additional phenotypes observed in *MAPT* V337M containing neurons and show that early phenotypes are due to a dominant negative tau loss of function caused by *MAPT* V337M and later phenotypes are caused by tau's toxic gain of function. We propose that pathogenic tau causes early loss of tau function in development, which contributes to the observed cognitive changes in preclinical *MAPT* gene carriers. As people age, pathogenic tau disrupts neuron and brain homeostasis via toxic gain of function, eventually causing neurodegeneration and disease.

RESULTS:

***MAPT* V337M and *MAPT* knockdown perturb transcription of axonogenesis genes**

iPSCs generated from a healthy individual (WTC11, referred to as *MAPT* WT) or an FTD patient with the *MAPT* V337M mutation (GIH6C1, referred to as **MAPT* Het) were edited in previous

work with Cas9 to generate isogenic pairs either introducing or correcting the *MAPT* V337M mutation (**Figure 1.1A**). The *MAPT* WT iPSCs were edited with Cas9 to generate a heterozygous *MAPT* V337M/WT clone (*MAPT* Het) and homozygous *MAPT* V337M/V337M clone (*MAPT* Hom). The **MAPT* Het iPSCs were corrected with Cas9 to generate a *MAPT* WT/WT clone (**MAPT* WT). We engineered the GIH6C1 lines to have a dox-inducible mNGN2 and to express CRISPRi machinery [25]. We transduced the iPSCs with lentiviral sgRNAs for further mechanistic characterization, such as non-targeting control (NTC) or *MAPT* sgRNAs to knock down tau.

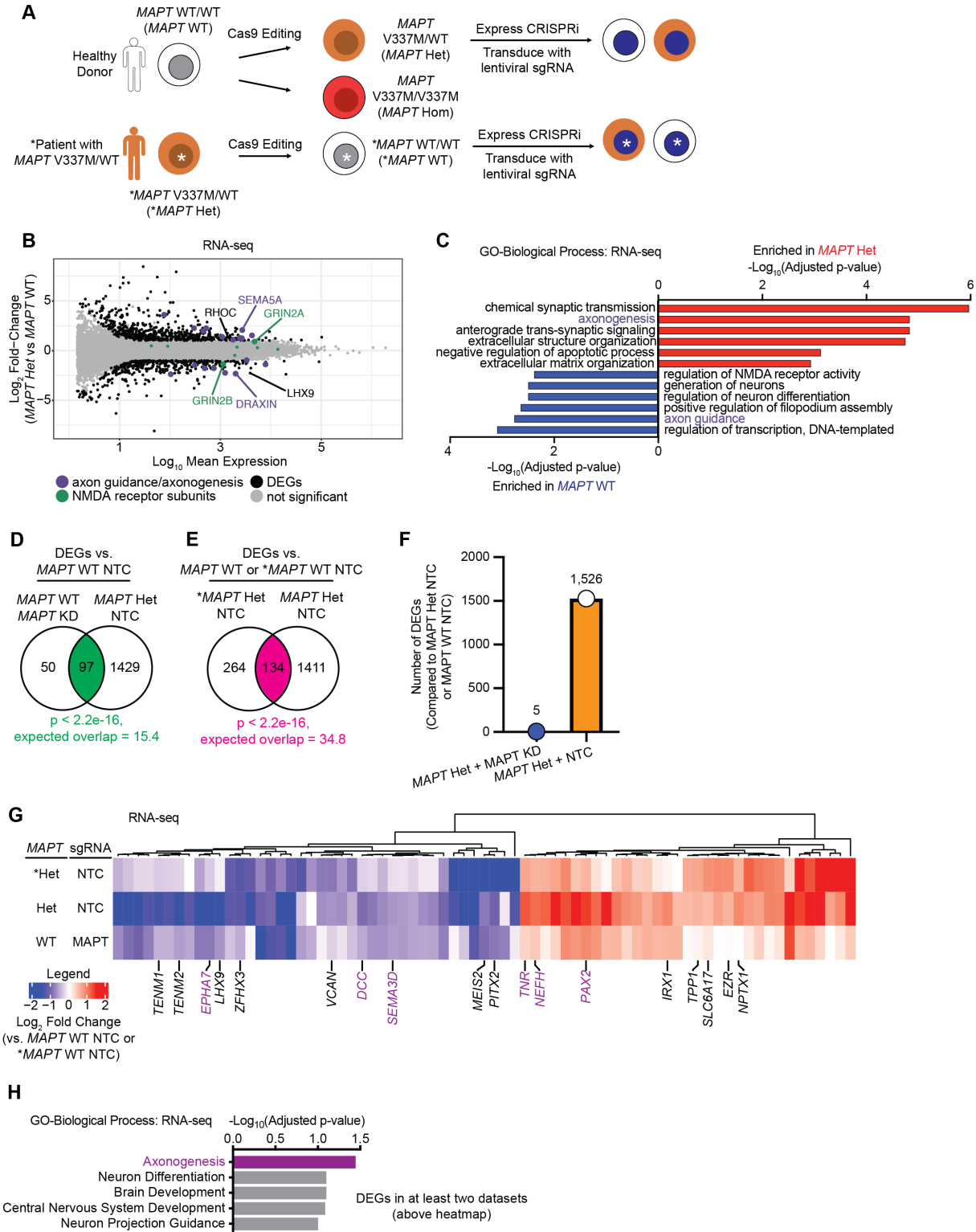


Figure 1.1: RNA-seq in MAPT V337M neurons reveals conserved changes in axonogenesis that mirrors tau reduction in MAPT WT neurons

(Figure caption continued on the next page)

(Figure caption continued from the previous page)

(A) (*Top Left*, iPSCs from a healthy donor (*MAPT* WT) were edited with Cas9 in previous work to generate a heterozygous *MAPT* V337M clone (*MAPT* Het) and a homozygous *MAPT* V337M clone (*MAPT* Hom). *Bottom Left*, iPSCs generated from a patient with the heterozygous *MAPT* V337M mutation (**MAPT* Het) were edited with Cas9 in previous work to generate a healthy isogenic control (**MAPT* WT). These cells were engineered to express a dox-inducible mNGN2 in the AAVS1 safe harbor locus and CRISPRi machinery in the *CLYBL* locus. We then transduce the iPSCs with lentivirus for sgRNA and BFP expression. **(B)** MA plot showing the change in gene expression between *MAPT* Het and *MAPT* WT neurons. Not significant genes are marked in grey, differentially expressed genes (DEGs) are marked with black circles. Genes in the axon guidance/axonogenesis GO terms are marked in purple, and NMDA receptor subunits are marked in green. **(C)** Gene Ontology (GO) term enrichment analysis of the RNA-seq experiment in (B). Genes enriched in *MAPT* Het are labeled in red, and genes enriched in *MAPT* WT are marked in blue. Terms involved in axonogenesis and axon guidance are colored purple. Top terms with minimal overlap are shown. **(D)** Overlap between DEGs in *MAPT* WT *MAPT* knockdown (KD) and *MAPT* Het NTC vs. *MAPT* WT NTC. Significance was calculated using Fisher's exact test. **(E)** Overlap between **MAPT* Het vs. *MAPT* WT and *MAPT* Het vs. *MAPT* WT. Significance was calculated as in (D). **(F)** Number of DEGs in *MAPT* Het *MAPT* KD vs. *MAPT* Het NTC and *MAPT* Het NTC vs. *MAPT* WT NTC. **(G)** Heatmap showing the log₂ fold changes of genes with differential expression in at least two of the three comparisons vs. *MAPT* WT NTC or **MAPT* WT NTC. Genes involved in axonogenesis are labeled in purple. **(H)** GO term enrichment of genes that are increased and decreased in the above heatmap. Axonogenesis is the only significant GO Biological Process term in this gene set. Top terms with minimal overlap are shown.

RNA-seq at day 14 of differentiation (**Figure 1.1B**) showed large changes in gene expression in *MAPT* Het vs. *MAPT* WT neurons. *GRIN2A* expression was elevated, and *GRIN2B* expression was decreased. The switch from *GRIN2B* expression to *GRIN2A* expression is a known developmental milestone [26]. We also observed changes in axon guidance and axonogenesis genes such as *SEMA5A* and *DRAXIN*. Gene set enrichment analysis emphasized the changes in synaptic and axon gene expression (**Figure 1.1C**).

We wanted to determine if the changes in gene expression were caused by a loss of tau function or a gain of a toxic function due to the mutation. We predicted that the gene expression changes would be due to a toxic gain of function of *MAPT* V337M based on previous work [17]. We

expected that knocking down tau in *MAPT* WT neurons would have almost no effect and knocking down tau in *MAPT* Het neurons would rescue gene expression, making it resemble *MAPT* WT. Intriguingly, knocking down tau in *MAPT* WT neurons caused significant changes in gene expression that substantially overlapped with the DEGs in *MAPT* Het and *Het neurons. The amount of overlap between DEGs in WT + *MAPT* knockdown (KD), Het and *Het neurons was much higher than would be expected by random chance (**Figure 1.1D,E**). This was surprising because previous reports in similar models found gain of function phenotypes caused by the *MAPT* V337M mutation [17], but our results suggest that tauopathy mutations can also cause loss of function phenotypes. There were many more DEGs in the *MAPT* Het neurons compared to the **MAPT* Het and *MAPT* WT *MAPT* knockdown neurons, which could reflect clonal differences between the iPSC lines or technical artifacts between the sample collection and sequencing.

Another surprise came when we looked at the effect of *MAPT* KD in *MAPT* Het neurons. Knocking down tau in *MAPT* Het neurons had almost no effect on transcription, with only 5 DEGs observed, also suggesting that the changes in gene expression are more likely due to a tau loss of function rather than a toxic gain of function (**Figure 1.1F**).

The differentially expressed genes that are shared between *MAPT* Het, **MAPT* Het and *MAPT* WT *MAPT* KD further emphasized the changes in genes regulating axonogenesis (**Figure 1.1G,H**). *EPHA7* and *DCC* are both receptors that facilitate axon guidance and cell-contact dependent signaling [27]. *SEMA3D* is a secreted ligand that serves as a repulsive signal, facilitating axon avoidance via growth cone pausing or collapse [27].

To uncover differentially regulated transcriptional regulators responsible for the DEGs we observed, we performed ATAC-seq on *MAPT* WT and *MAPT* Het neurons at day 14 of differentiation with NTC or *MAPT* sgRNAs. ATAC-seq revealed many changes in chromatin accessibility that roughly clustered into three categories (**Figure 1.2A**). The first cluster is mostly comprised of regulators of neuron differentiation, including three members of the POU class 4 transcription factors. Motifs associated with POU class 4 transcription factors were more accessible in both *MAPT* Het NTC and *MAPT* WT tau knockdown neurons compared to *MAPT* WT NTC neurons. The second cluster is comprised of members of the AP-1 transcription factor network, such as *FOS* and *JUN*. These motifs were more accessible in the *MAPT* Het neurons. The accessibility of AP-1 transcription factor motifs was not changed in *MAPT* WT tau knockdown neurons compared to controls. The third cluster is comprised of genes that regulate the response to oxidative stress, such as *NFE2L1* and *NFE2L2*. These motifs were also more accessible in *MAPT* Het neurons compared to *MAPT* WT neurons. Interestingly, three early B-cell factor (EBF) transcription factor motifs showed increased accessibility in both *MAPT* Het and *MAPT* WT tau knockdown neurons.

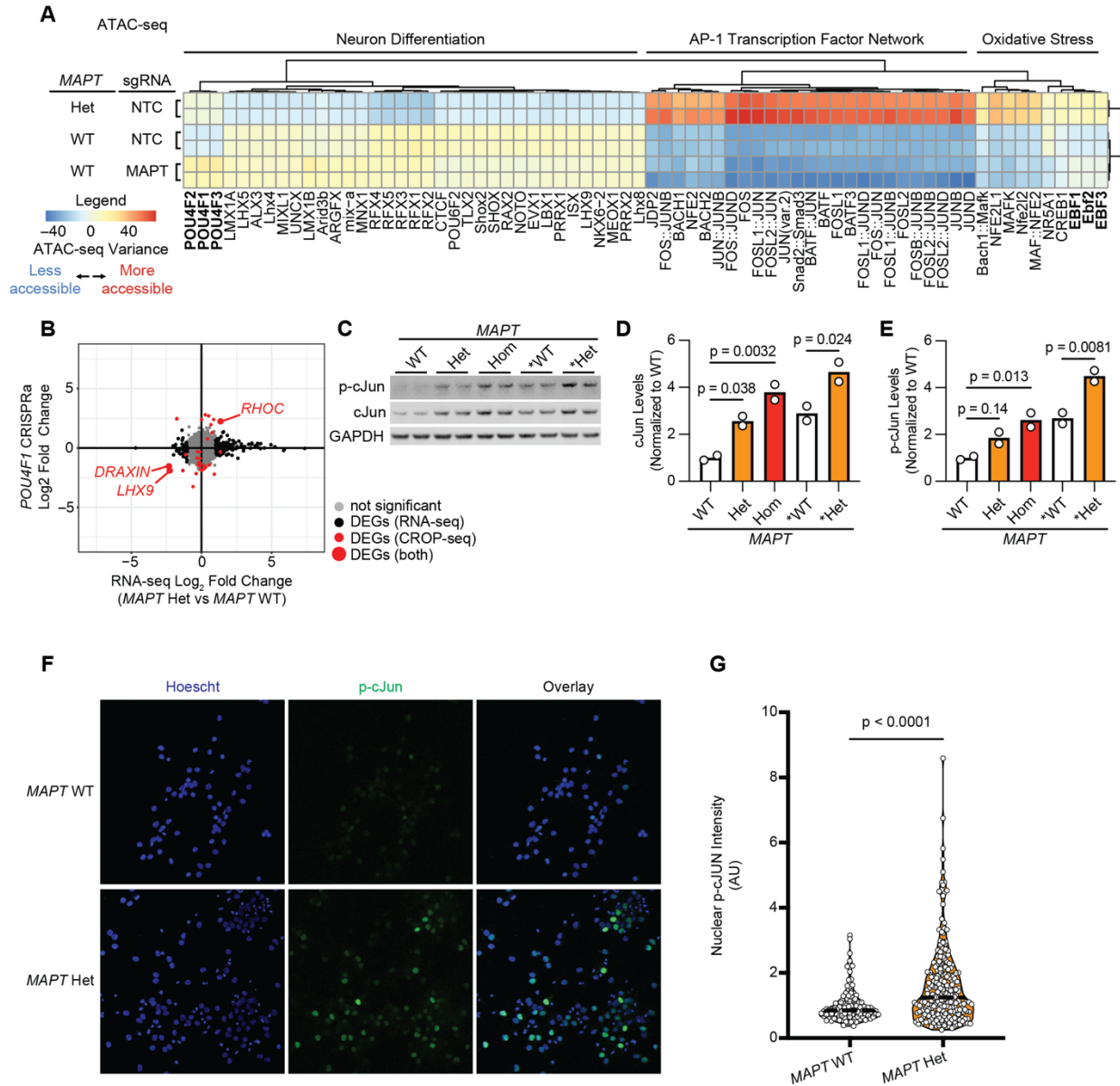


Figure 1.2: ATAC-seq uncovers tau dependent and independent regulators of gene expression in MAPT Het, MAPT WT and MAPT WT tau knockdown neurons

(A) Heatmap summarizing ATAC-seq data from *MAPT* Het, *MAPT* WT NTC and *MAPT* WT *MAPT* KD neurons. ATAC-seq variance is represented, with blue or negative values reflecting less accessible chromatin and red or positive values reflecting more accessible chromatin.

Transcription factor motifs that were different in at least one condition were clustered, and GSEA was performed on the clusters to approximate the function of transcription factors in each cluster. Bolded transcription factors (*POU4F1*, *POU4F2*, *POU4F3*, *EBF1*, *EBF2*, *EBF3*) showed consistent phenotypes in both *MAPT* Het and *MAPT* WT *MAPT* KD neurons, suggesting that these transcription factors could represent a response to tau loss of function.

(Figure caption continued on next page)

(Figure caption continued from previous page)

(B) Analysis of CROP-seq data from Tian et al. 2021 [28]. DEGs in the *POU4F1* CRISPRa neurons were compared to DEGs in the RNA-seq of *MAPT* Het NTC vs. *MAPT* WT NTC. DEGs in the RNA-seq are represented by black dots, and DEGs in the CROP-seq experiment are represented with red dots. DEGs in both experiments are labeled in red. **(C)** Western blot measuring p-cJun and cJun levels in *MAPT* V337M vs *MAPT* WT neurons. **(D-E)** Quantification of cJun (D) and p-cJun (E) from the western blot in (C). Bars represent the mean of 2 data points. Significance was calculated using one-way ANOVA with Dunnett's multiple comparison test, and comparisons were restricted within the donor background. **(F)** Representative images of Hoescht (*left, blue*) p-cJun, (*center, green*), and overlaid images (*right*). **(G)** Quantification of nuclear p-cJun intensity. Significance was calculated using an unpaired t test. Each point represents a single cell, and the median is shown as a dotted black line.

We previously performed CROP-seq on neurons on day 10 of differentiation using both CRISPRa and CRISPRi perturbing the *POU4F1* gene [28]. This allowed us to survey the effects of both gene knockdown and overexpression in our neurons to uncover which DEGs were likely influenced by changes in *POU4F1* activation. The majority of genes modified by *POU4F1* perturbations are involved in axonogenesis (**Figure 1.2B**). *DRAXIN* and *LHX9* both regulate axonogenesis and were DEGs in both the *MAPT* Het neurons as well as the *POU4F1* CROP-seq.

Since *JUN* regulates its own expression, we hypothesized that increased *JUN* accessibility would lead to increased cJun protein levels. The V337M mutation caused increased cJun levels in *MAPT* Het, Hom and *Het neurons compared to *MAPT* WT or *WT neurons at day 7 of differentiation (**Figure 1.2C-E**). There was also increased nuclear phospho-cJun in *MAPT* Het neurons compared to *MAPT* WT neurons (**Figure 1.2F-G**), which is consistent with the increased activation of cJun activity. The transcriptomic data suggest that *MAPT* V337M and *MAPT* knockdown drive conserved changes in the expression of axonogenesis genes.

***MAPT* V337M perturbs levels and phosphorylation of axonogenesis proteins**

cJun activity and nuclear localization are regulated by MAP kinase signaling. We wanted to test changes that the V337M tau mutation might cause to cellular signaling pathways with an unbiased method. Total proteomics and phosphoproteomics were conducted on day 7 neurons in both *MAPT* Hom vs WT and *MAPT* *Het vs *WT neurons. There were 202 proteins with significantly different levels in neurons with the *MAPT* V337M mutation (**Figure 1.3A**). Of these, 92 proteins were changed in the same direction in both the healthy donor and patient derived neurons. Closer examination of these hits again revealed consistent changes in proteins that regulate axonogenesis (**Figure 1.3B-C**). *GSK3B* and *APOE* levels were both changed, and they are both regulators of axon extension as well as known regulators of tauopathy in Alzheimer's disease. Many of the significantly changed proteins were also RNA binding proteins (**Figure 1.3D**).



Figure 1.3: Proteomics shows convergence on altered regulation of axonogenesis protein levels and phosphorylation in neurons with *MAPT* V337M
(Figure caption continued on the next page)

(Figure caption continued from the previous page)

(A) Overlap between the proteomics datasets in *MAPT* Hom vs. *MAPT* WT neurons and **MAPT* Het vs. **MAPT* WT neurons. Significance was calculated using Fisher's Exact test. Significantly differential proteins in both datasets were subsequently filtered to identify proteins with consistent phenotypes in both datasets, and this subset of 92 hits was used for subsequent analysis. **(B)** Heatmap showing the Log_2 fold change of protein abundance in *MAPT* Hom or **Het* neurons vs. *MAPT* WT or **WT* neurons. Proteins annotated in the Regulation of axon extension term were labeled in purple, proteins in the RNA binding term are labeled green. Proteins that are annotated to have tau protein binding activity are annotated with a pink circle next to their gene name. **(C-D)** GO term enrichment of proteins with differential abundance in both *MAPT* Hom and **Het* neurons compared to controls. Top terms with minimal overlap are shown. Term names are colored to match relevant gene names in the above heatmap. "Hydrolase activity, acting on carbon-nitrogen (but not peptide) bonds, in linear amidines" was abbreviated to "Hydrolase activity..." **(E)** Volcano plot showing changes in protein phosphorylation in *MAPT* Hom vs. *MAPT* WT neurons. Proteins are color-coded based by pathways based on GO annotation. **(F)** GO term enrichment of differentially phosphorylated proteins from (E). Proteins with higher phosphopeptide abundance in *MAPT* Hom are colored in red, and proteins with lower phosphopeptide abundance in *MAPT* Hom are colored blue. Terms that are related to axonogenesis are colored in purple. The top ten terms are displayed for each category. **(G)** (*Top*) Overlap between differential phosphosites in *MAPT* Hom and **Het* neurons vs controls. Significance was calculated using Fisher's Exact Test. (*Bottom*) Overlap between proteins with differential phosphorylation in both datasets. Significance was calculated using Fisher's Exact Test. **(H)** GO term enrichment analysis on conserved proteins with differential phosphorylation in *MAPT* Hom and **Het* neurons vs. controls. Terms related to axonogenesis are colored purple. "Plasma Membrane Bounded Cell Projection Organization" was abbreviated to "Cell Projection Organization" and "Negative Regulation of Axonogenesis" was abbreviated to "Neg. regulation of Axonogenesis." **(I)** Kinase activity analysis from *MAPT* Hom vs. *MAPT* WT phosphorylation changes. The log_2 fold change of phosphopeptide abundance for annotated kinase substrates is plotted. The significance is calculated based on the number of known substrates and how many substrates are modified in the same direction. The range is represented by the thin lines, the box represents the IQR, and the median is represented by a thick line. **(J)** Kinase activity scores from both datasets. Significant kinases in **MAPT* Het are marked in red, significant kinases in *MAPT* Hom are marked in blue, and kinases significant in both datasets are marked in purple. **(K)** Mapping differential phosphorylations onto a protein domain map of *MAPIB*. (*Left*), differential phosphorylations are marked with a black line with an open circle on top, non-differential phosphorylations are marked with just a black line below the domain map. Within the open circle on significantly differential phosphorylations, the top half is the phenotype in *MAPT* Hom vs. WT and the bottom half is the phenotype in **MAPT* Het vs. **WT* neurons. Abbreviations for domains are as follows: Acin binding domain (ABD), Light chain 1 interaction (LC1 Interaction), Microtubule binding domain (MBD), Light Chain 1 (LC1). An annotated nitrosylation (NO) is shown in yellow at the c-terminus of the protein.

The phosphoproteomics were also enriched for modifiers of axonogenesis (**Figure 1.3E,F**). Many of the phosphosites that were significantly increased in *MAPT* Hom vs. *MAPT* WT were phosphosites on RNA splicing proteins, including *HNRNPA2B1*, *HNRNPH1*. p-cJUN was significantly increased, and phosphorylation of some regulators of axonal transport was also increased. The proteins with decreased phosphorylation in *MAPT* Hom neurons were regulators of axonogenesis, including *MAP1B*, *MAPT*, *DCLK* and *MAP2*. *DPYSL3* and other Collapsin Response Mediator Proteins (CRMPs) were also dephosphorylated. CRMPs mediate cytoskeletal reorganization in response to class 3 semaphorin signaling [29]. There was little overlap between the differential phosphosites in the *MAPT* Hom and **MAPT* Het datasets (**Figure 1.3G**). There were fewer significant differential phosphosites in the **MAPT* Het dataset, and overall there was less coverage in this dataset. Despite this, we see a significant overlap between the datasets when we look at proteins that have differential phosphorylation. The 89 conserved proteins between the datasets with differential phosphorylation are highly enriched for proteins that regulate axonogenesis (**Figure 1.3H**).

We then aggregated the phosphorylation sites by the kinases predicted to act on them to identify kinases that were significantly enriched for having increased or decreased activity in *MAPT* Hom neurons (**Figure 1.3I**). CDK5R1, a regulator of CDK5 that has important roles in neuronal development and axonogenesis, had significantly decreased levels of phosphorylation for its substrates. Additionally, CSNK1E and CSNK2B had decreased activity. Kinases in the p38 MAP kinase pathway were highly represented in the kinases that were predicted to have higher activity. MAP2K3 and MAP2K6 are both MAP2K's that phosphorylate p38 MAPK. The p38 MAP kinase pathway is canonically known as a stress response, but also plays an important role

in synaptic signaling and plasticity [30, 31]. *CDK5* and *CDK5RI*, though not significant in both datasets, clearly are the major predicted upstream kinases for substrates with decreased phosphorylation in neurons with the *MAPT* V337M mutation (**Figure 1.3J**). Additionally, several regulators of the p38 MAPK pathway were also conserved in both datasets, including *MAP2K3* and *MAP2K6*.

One example of a *CDK5* substrate that is a key regulator of axonogenesis and axon guidance is *MAP1B*. *MAP1B* is a microtubule and actin-binding protein that plays important roles in growth cone dynamics. *MAP1B* protein levels were decreased (**Figure 1.3B**) and several phosphosites were decreased in both datasets (**Figure 1.3K**). We mapped the phosphosites and differential phosphosites on the *MAP1B* domain annotations from Uniprot [32]. The specific phosphosites did not match between the two isogenic pairs of cells. All the significantly differential *MAP1B* phosphosites had decreased phosphorylation in both datasets. Many of the significantly different phosphosites map to a disordered region around 1244-1276. This region is known to be regulated by *GSK3B* and *CDK5* and has been shown to be enriched in serines and threonines that can be phosphorylated by *GSK3B* without priming [33]. Importantly, *MAP1B* phosphorylation by *GSK3B* has been shown to regulate axonogenesis and specifically axon branching in recent work [34, 35]. The proteomics and phosphoproteomics show that both transcriptomic and post-translational changes point to altered axonogenesis in that *MAPT* V337M neurons.

***MAPT* V337M causes axon branching due to tau loss of function**

To directly test how the *MAPT* V337M mutation perturbs axonogenesis, we longitudinally imaged neurons expressing a membrane-targeted Lck-mNeonGreen and a nuclear localized NLS-mTagBFP (**Figure 1.4A**). Images were blinded and manually traced to measure axon, axon branch and secondary neurite length over time. By day 3 post differentiation, surviving neurons begin to polarize and form a main axon (**Figure 1.4B**). Strikingly, beginning around day 5, neurons expressing tau with the V337M mutation began to have extensive axon branching compared to the *MAPT* WT and *WT control neurons. Total neurite length was not substantially altered between the lines over time (**Figure 1.4C**), nor was the length of the main axon (**Figure 1.4D**). However, axon branch length was clearly altered beginning at day 5 and continuing through day 11 (**Figure 1.4E, G-I**). Intriguingly, the *MAPT* Hom neurons with two copies of mutant tau also seemed to have a higher propensity for more than one long axon in addition to increased axon branching, though the increased axon branching takes longer than in *MAPT* Het neurons. (**Figure 1.4F, J**).

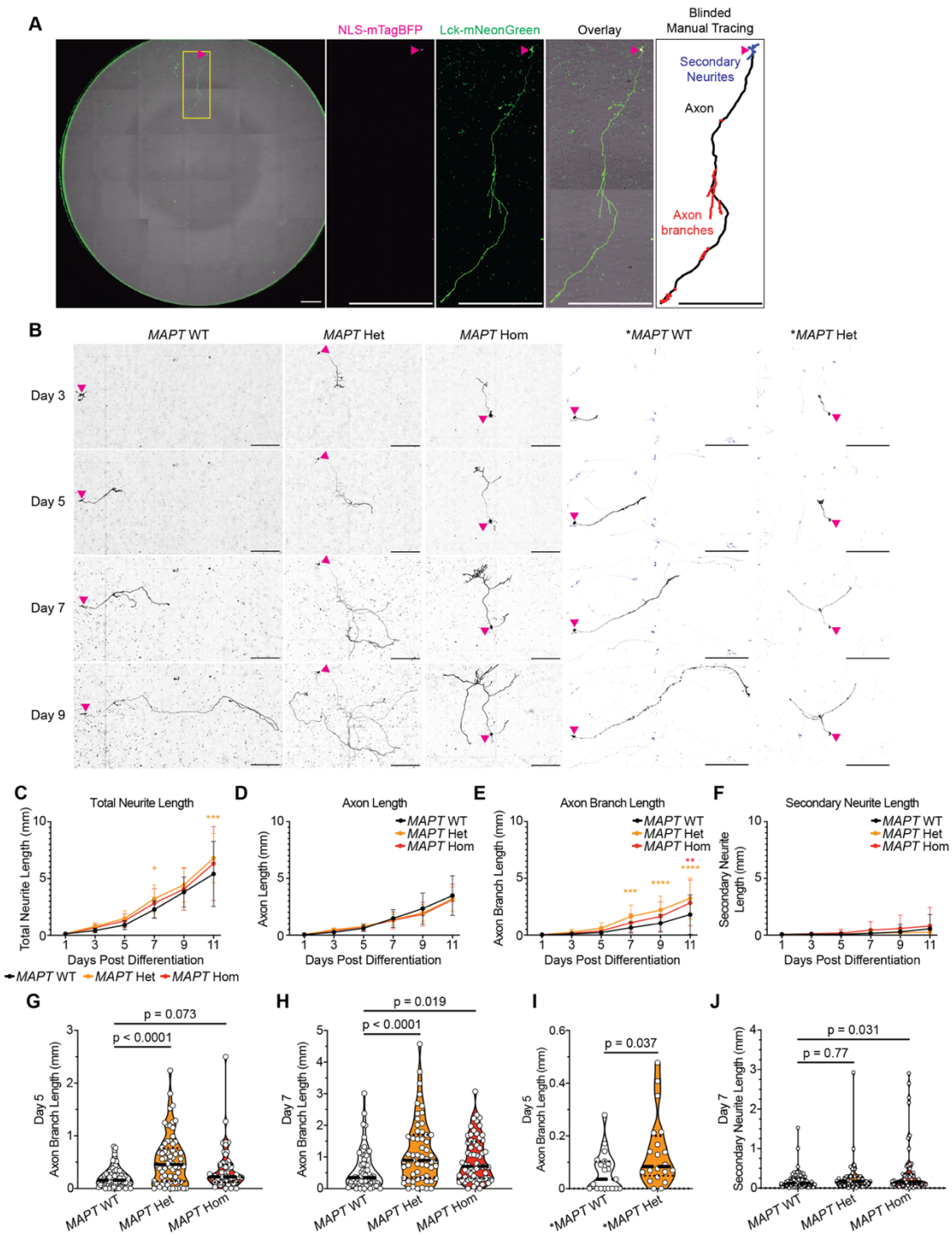


Figure 1.4: MAPT V337M induces axon branching in differentiating neurons without substantially perturbing other parameters of neurite outgrowth

(Figure caption continued on the next page)

(Figure caption continued from the previous page)

(A) (From left) Entire well of a 96 well stitched together and overlaid. The nucleus is marked with a magenta arrowhead, and the inset region of interest (ROI) is marked with a yellow box. In all images, the scale bar is 500 μ m. NLS-mTagBFP (magenta) marks the nucleus (magenta arrowhead). Lck-mNeonGreen (green) labels the soma, axon and secondary neurites. Overlay showing the sparse labeled neuron with many unlabeled neurons close by. Example inset of a manually traced neuron showing the features measured. **(B)** Representative images of neurons expressing Lck-mNeonGreen (black) over time. Soma are marked with magenta arrowheads, and the scale bar is 500 μ m. **(C)** Total neurite length, or the sum of the axon length, the axon branch lengths and the secondary neurite lengths, was quantified at each timepoint. The mean and standard deviation are plotted. Significance was calculated using two-way ANOVA with Dunnett's multiple comparisons test. * $p = 0.016$ and *** $p = 0.0009$. **(D)** Axon length measured over time. The axon was determined to be the longest primary neurite extending from the soma. No significant differences were observed. The mean and standard deviation are plotted. **(E)** Axon branch length over time. Axon branches were determined to be neurites that branched from the primary main axon. The mean and standard deviation are plotted. Day 7 ***: $p = 0.0001$, Day 9 ****: $p < 0.0001$, Day 11 ** $p = 0.0018$, Day 11 **** $p < 0.0001$. **(F)** Secondary neurite length over time. Secondary neurites are neurites that extend from the soma itself but are not the longest or primary axon. These likely include dendrites as well as additional axons in bipolar or multipolar neurons. The mean and standard deviation are plotted. **(G)** Axon branch length at day 5. Significance for this and subsequent single timepoint analyses were calculated using one-way ANOVA with Dunnett's multiple comparisons test. The thick lines represent the median, and the tinner dashed lines represent the IQR. **(H)** Day 7 of differentiation axon branch length. The thick lines represent the median, and the tinner dashed lines represent the IQR. **(I)** Day 5 axon branch length in **MAPT* Het and *MAPT* WT neurons. The thick lines represent the median, and the tinner dashed lines represent the IQR. **(J)** Day 7 secondary neurite length. The thick lines represent the median, and the tinner dashed lines represent the IQR.

We next wanted to determine if the axon branching phenotype was due to a toxic gain of function of the mutant tau or a loss of function. We looked for regulators of axonogenesis and cytoskeletal dynamics from tau interactome data using the V337M mutation in iPSC-derived neurons [24].

This work showed that *MYO1B*, a known regulator of actin and filopodia stability in developing axons [36], was a top increased interactor with both V337M and P301L tau in iPSC-derived neurons (**Figure 1.5A**). Knocking down tau and *MYO1B* in *MAPT* WT neurons induced extensive axon branching like what is observed in *MAPT* V337M neurons (**Figure 1.5D-F**).

Knocking down tau and *MYO1B* in *MAPT* V337M neurons did not modify the axon branching

phenotype. These data strongly support the *MAPT* V337M mutation causing tau loss of function in differentiating neurons.

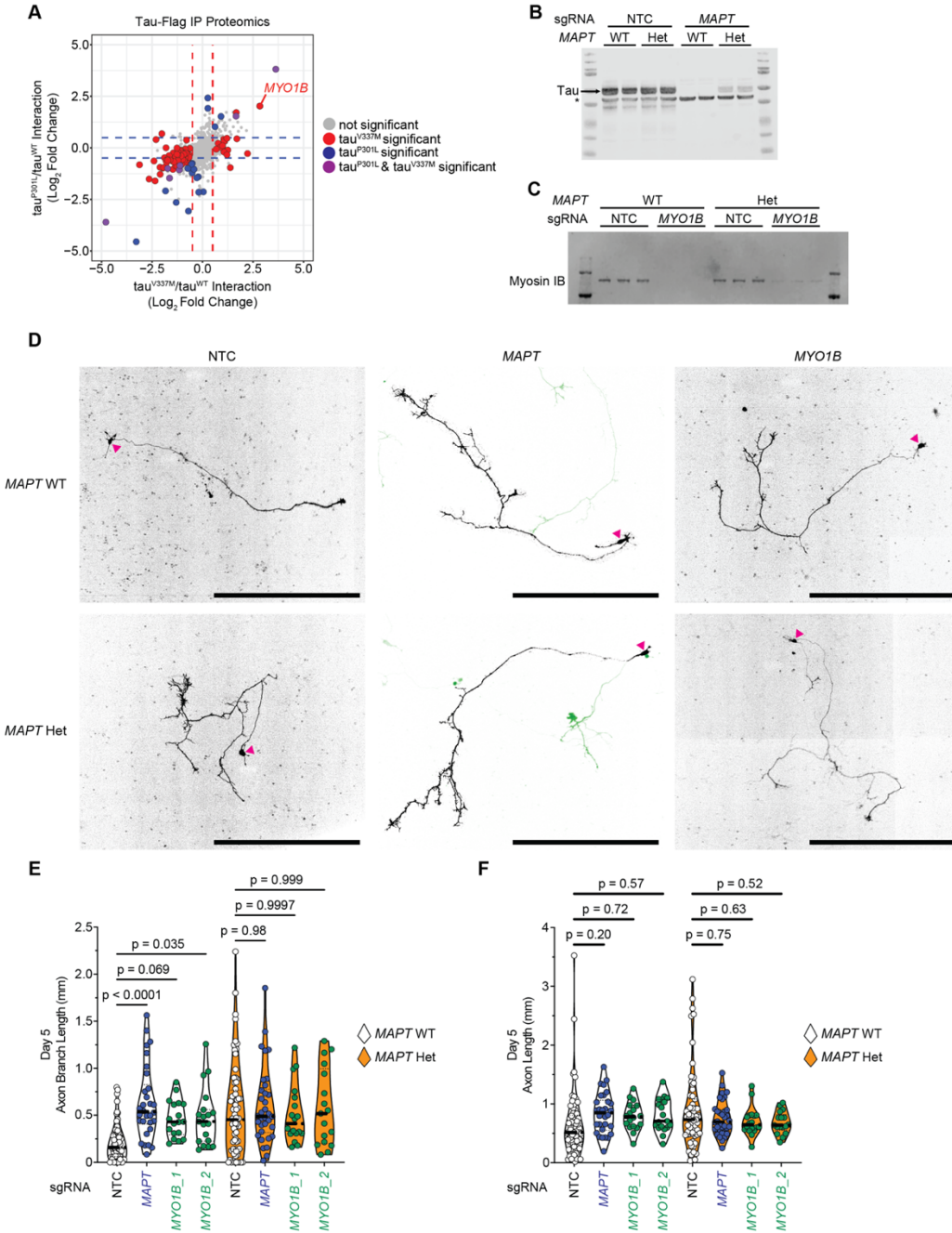


Figure 1.5: MAPT knockdown and MYO1B knockdown induce axon branching in MAPT WT neurons

(Figure caption continued on the next page)

(Figure caption continued from the previous page)

(A) Tau-Flag IP proteomics data from Tracy et al. [24]. Not significantly different tau interactors were colored in grey, significant tau^{V337M} interactors are colored in red, significant tau^{P301L} interactors are colored in blue and interactors that are significantly different in both datasets are colored in purple. Dashed lines represent +/- 0.5 log₂ fold change to help visualize approximate significance cutoffs. Significance was calculated by multiplying the log₂ fold change by the log₁₀ adjusted p value to calculate an enrichment score. **(B)** Western blot showing robust tau knockdown in neurons with an sgRNA targeting *MAPT*. Tau is annotated with a label and black arrow, and a non-specific band is marked with an asterisk. **(C)** Western blot showing robust *MYO1B* knockdown in neurons with sgRNAs targeting *MYO1B*. **(D)** Representative images of Lck-mNeonGreen labeled neurons (Black) with NTC, *MAPT* or *MYO1B* sgRNAs. Scale bar is equal to 500µm. Soma are marked with a magenta arrowhead. The neurons containing the *MAPT* sgRNA had other labeled neurons crossing into the image. To emphasize the representative neuron, the focused neuron was cropped and displayed in black, and background labeled neurons are displayed in green (*center*). **(E)** Quantification of axon branch length at day 5 of differentiation. The thick lines represent the median, and the tinner dashed lines represent the IQR. Significance was calculated using one-way ANOVA with Dunnett's multiple comparisons test in (E) and (F). **(F)** Day 5 Axon length was not significantly changed in *MAPT* knockdown or *MYO1B* knockdown neurons.

***MAPT* V337M neurons have decreased viability and mitophagy**

To untangle the potential loss of function and gain of function effects of *MAPT* V337M, we characterized additional phenotypes in our neurons. Neurons containing the *MAPT* V337M mutation had decreased viability over time (**Figure 1.6A-D**). We also checked the sensitivity of *MAPT* WT and *MAPT* Het neurons to mitochondrial stress by treating with the ATP synthase inhibitor oligomycin. *MAPT* Het neurons were hypersensitive to oligomycin treatment in anti-oxidant free media at day 14 of differentiation. Intriguingly, tau knockdown partially rescued oligomycin hypersensitivity in *MAPT* Het neurons, suggesting a gain of function effect of *MAPT* V337M.

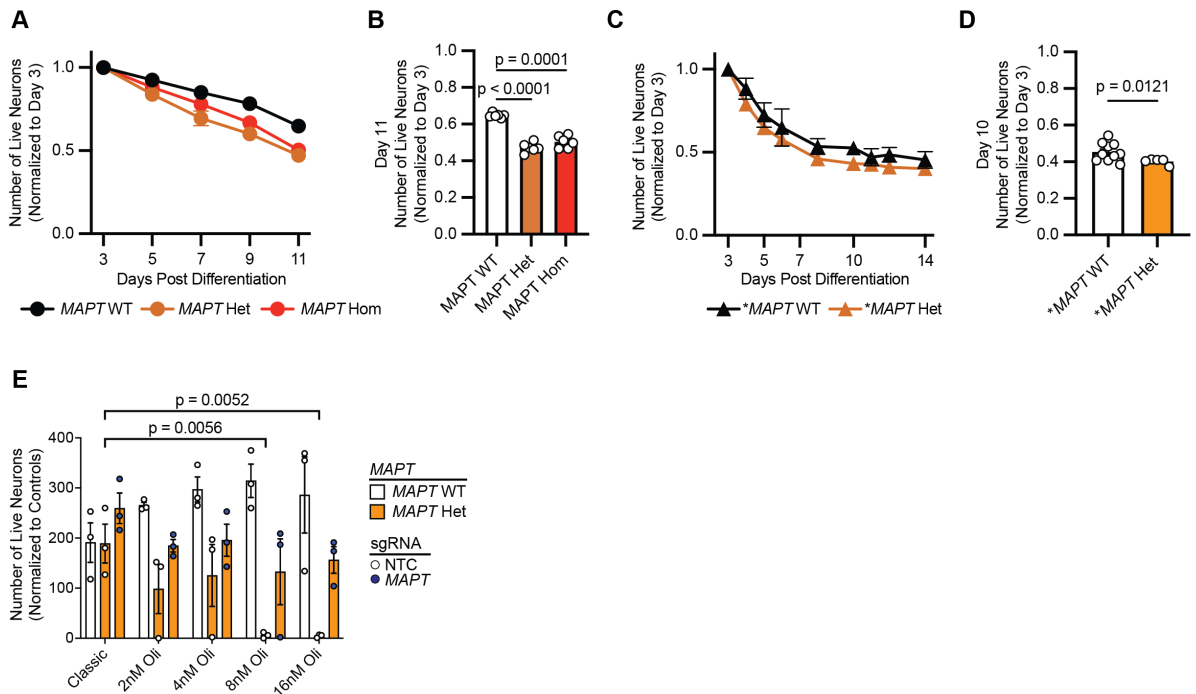


Figure 1.6: MAPT V337M causes toxicity and hypersensitivity to mitochondrial stress

(A,C) Neuron survival was measured over time by imaging NLS-mTagBFP and Topro3 iodide, a cell membrane impermeable dye that is taken up into dying cells and fluoresces upon binding DNA. The number of viable cells was calculated each day and normalized to the number of neurons on day 3. The mean and standard error of the mean are plotted over time. (B) The number of live neurons on day 11 normalized to day 3. Significance was calculated by one-way ANOVA with Dunnett's multiple comparison test. The mean and standard error of the mean are plotted. (D) The number of live neurons on day 10 normalized to day 3. Significance was calculated with an unpaired t test. The mean and standard error of the mean are plotted. (E) Oligomycin hypersensitivity was measured in *MAPT* WT and *MAPT* Het neurons with NTC sgRNA or *MAPT* sgRNA (in *MAPT* Het neurons). Significance was calculated using one-way ANOVA with Dunnett's multiple comparisons test. The mean and standard error of the mean are plotted.

Total proteomics on day 28 *MAPT* Het neurons vs. *MAPT* WT neurons revealed consistent increases in mitochondrial proteins (Figure 1.7A). Gene set enrichment analysis showed that most of these proteins were involved in the electron transport chain (ETC) or ETC assembly (Figure 1.7B). We validated the accumulation of mitochondrial proteins at day 14 of differentiation by western blot and showed that neurons with the *MAPT* V337M mutation have

increased mitochondrial protein levels (**Figure 1.7 C-F**). Comparing the proteomics at day 28 to RNA-seq at day 28 showed that the increased mitochondrial protein levels do not correlate with increased expression of their transcripts (**Figure 1.7G**). *MAPT* Het neurons also did not have increased RNA levels of mitochondrial transcripts at earlier timepoints (day 7 and day 14 of differentiation, data not shown). We hypothesized that the accumulation of mitochondrial proteins was likely due to decreased mitophagy. We validated changes in mitophagy in our neurons using the mitophagy reporter mt-Keima, a fluorescent protein that has different excitation wavelengths depending on pH [37]. *MAPT* Het neurons had a decreased mtKeima ratio, consistent with lower levels of mitophagy ongoing relative to *MAPT* WT neurons (**Figure 1.7H**).

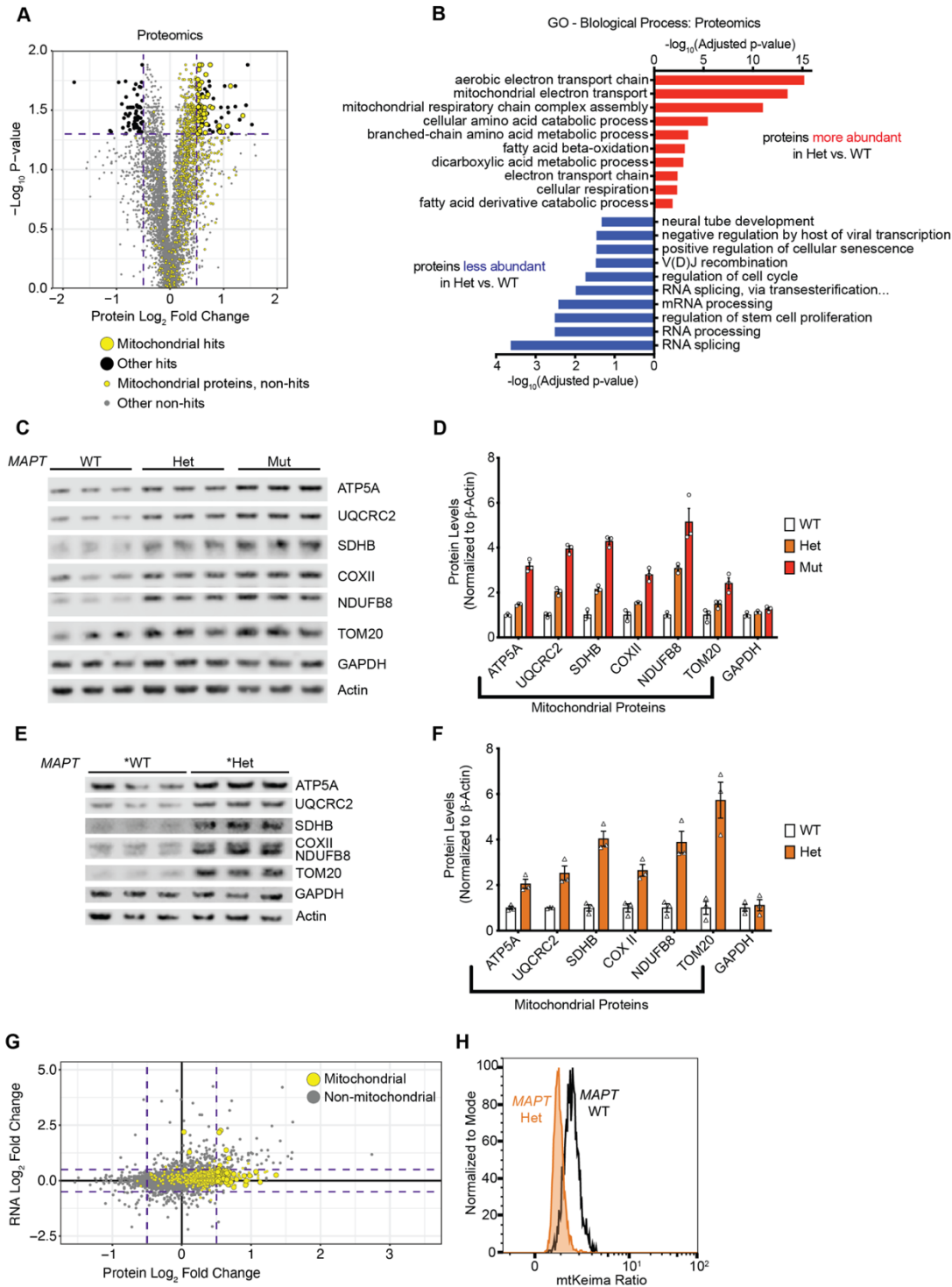


Figure 1.7: MAPT V337M neurons have increased mitochondrial protein levels and decreased mitophagy

(Figure caption continued on the next page)

(Figure caption continued from the previous page)

(A) Volcano plot showing total proteomics of *MAPT* Het neurons compared to *MAPT* WT neurons at day 28 of differentiation. Purple dashed lines show the significance cutoff (\log_2 fold change = +/-0.5, $-\log_{10}$ p-value > 1.30103). Mitochondrial proteins are showed with yellow circles, significantly differential proteins are shown in black, non-significantly differential proteins are shown in grey. (B) GO term enrichment analysis. Top 10 terms for proteins that are more abundant or less abundant in *MAPT* Het vs WT are displayed. (C,E) Western blot validating increased mitochondrial protein levels in *MAPT* V337M containing neurons. (D,F) Quantification of western blots in (C,E). Significance was calculated using two way ANOVA with Dunnett's multiple comparisons test. The mean and standard error of the mean are plotted. (G) Protein abundance was compared to RNA abundance in day 28 of differentiation comparing *MAPT* Het vs. WT neurons. Mitochondrial proteins are displayed in yellow. Purple dashed lines are displayed to help visualize significance cutoffs. (H) Representative histogram showing decreased mitophagy in *MAPT* Het neurons.

***MAPT* V337M causes loss of function phenotypes early during differentiation followed by gain of function phenotypes**

We wanted to determine the effect of reducing tau levels on these phenotypes and then see if overexpressing tau^{WT} or tau^{V337M} can rescue or induce these phenotypes (**Figure 1.8A**). We expressed GFP, GFP N-terminally tagged tau^{WT} or GFP-tau^{V337M} in *MAPT* WT neurons with tau knockdown (**Figure 1.8A-C**). As expected, we detected GFP, tau and GFP-tau bands in these cells (**Figure 1.8B**). Imaging showed nucleocytoplasmic localization of GFP that was enriched in the soma and microtubule localization of GFP-tau (**Figure 1.8C**).

Overexpressing GFP-tau^{V337M} caused increased mitochondrial proteins similar to what is observed in *MAPT* Het, *MAPT* Hom or **MAPT* Het compared to their isogenic controls (**Figure 1.8D,E**). However, when we used Cas9 to create tau knockout lines, we observed that knocking out tau did not perturb mitochondrial protein levels in *MAPT* WT or *MAPT* Het neurons (**Figure 1.8F**). There is a lot of evidence supporting mutant tau perturbing mitochondrial biology. But in

our system, it is unclear if the decrease in mitophagy is a toxic gain of function or simply a clonal effect that happened to occur.

MAPT knockdown did not rescue the survival defect in *MAPT* Het neurons, and in *MAPT* WT neurons it may even cause some toxicity (**Figure 1.8G**). *MAPT* knockdown and *MYO1B* knockdown did not substantially alter survival in *MAPT* WT or *MAPT* Het neurons (**Figure 1.8H**). *MYO1B* knockdown did not modify cJun protein levels (**Figure 1.8I,J**) or mitochondrial protein levels (**Figure 1.8K**). Since *MYO1B* knockdown induces axon branching but does not modify survival, cJun protein levels or mitochondrial accumulation in *MAPT* WT neurons, axon branching is not sufficient to induce these other phenotypes in the absence of pathogenic tau.

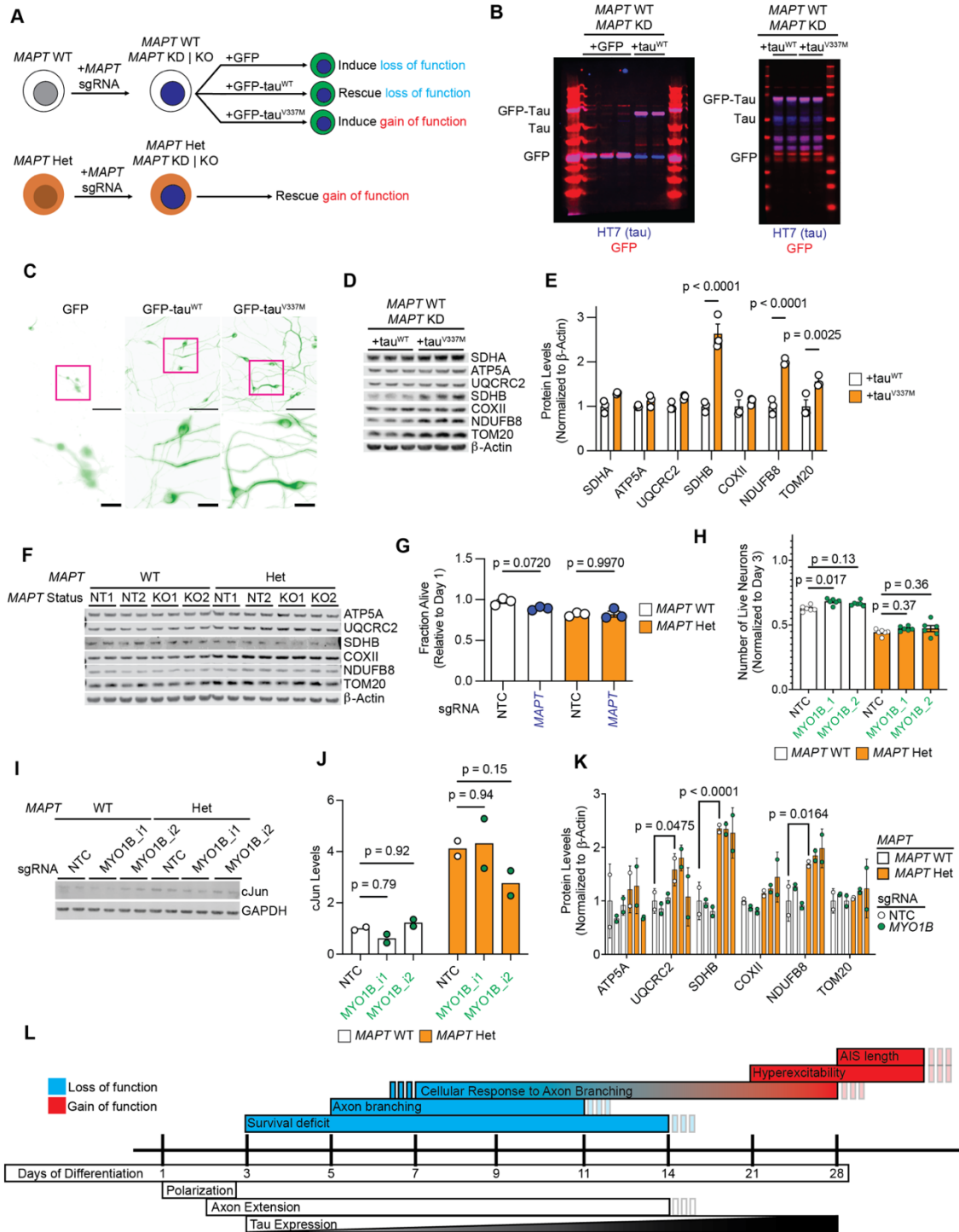


Figure 1.8: MAPT V337M perturbs neurons via tau loss of function and tau gain of function

(Figure caption continued on the next page)

(Figure caption continued from the previous page)

(A) Overview of expected outcomes in tau reduction and supplementation. **(B)** Western blots showing GFP, GFP-tau^{WT} and GFP-tau^{V337M} expression. **(C)** Representative images of neurons expressing GFP (*left*), GFP-tau^{WT} (*center*), and GFP-tau^{V337M} (*right*). Scale bars are equal to 100µm (*top*). Inset ROIs are marked with magenta boxes. Inset scale bars are equal to 25µm. **(D)** Western blot comparing mitochondrial protein levels in *MAPT* WT neurons expressing tau^{WT} and tau^{V337M}. **(E)** Quantification of (D). Significance was calculated using one-way ANOVA with Dunnett's multiple comparisons test. The mean and standard error of the mean are plotted. **(F)** Western blot of mitochondrial proteins in tau knockout neurons and unedited controls. **(G)** Effect of *MAPT* knockdown on viability. Significance was calculated using one-way ANOVA with Dunnett's multiple comparisons test. The mean and standard error of the mean are plotted. **(H)** Effect of *MYO1B* knockdown on viability. Significance was calculated using one-way ANOVA with Dunnett's multiple comparisons test. The mean and standard error of the mean are plotted. **(I)** Western blot for cJun levels with NTC sgRNAs or *MYO1B* sgRNAs. **(J)** Quantification of western blot in (I). Significance was calculated using one-way ANOVA with Dunnett's multiple comparisons test. The mean of two data points is represented by the bars. **(K)** Mitochondrial protein levels were quantified by western blot (not shown) in neurons with *MYO1B* knockdown. Significance was calculated using two-way ANOVA with Dunnett's multiple comparisons test. The mean and standard error of the mean are plotted. **(L)** Model of phenotypes identified in this study and in other studies using our model system. Early phenotypes in *MAPT* V337M are driven by tau loss of function, and later phenotypes are driven by tau gain of function. Typical timing for phenotypes in normal differentiation are annotated below the timeline. Smaller bars indicate that phenotypes may extend beyond what was measured in our study and others.

Our work has uncovered that early during the NGN2 neuron differentiation, the *MAPT* V337M mutation has a dominant negative loss of function effect on both survival and premature axon branching (**Figure 1.8L**). As the neurons continue to mature, the gain of function effects of *MAPT* V337M drive later phenotypes, including hyperexcitability and disrupted AIS plasticity [17].

DISCUSSION:

We have discovered that an FTD variant of tau causes loss of tau function in regulating axonogenesis in differentiating neurons.

Other groups have shown, mostly in mice or in primary neurons, that reducing tau can have varying effects on axonogenesis. Acute tau ablation in mouse neurons *in vitro* prevents axonogenesis by inhibiting polarization [38, 39]. Another group showed that in primary hippocampal neurons tau knockout reduces neurite outgrowth and branching, contrary to our findings [40]. There are several differences between our model and their systems that could explain this discrepancy. Our neurons are human and are derived from a transcription factor-based differentiation in the absence of glia or the context of the brain. We also measured our axon branching at later timepoints than what was done in these earlier papers, in part because our sparse plating approach with fluorescently labeled neurons allowed us to monitor individual neuron morphogenesis for much longer and in the presence of many unlabeled cells, which may improve neuronal health. We also observed that the plating conditions have a large impact on the outcome of these assays. Commercially coated plates purchased from Corning had the best overall performance in axon stability, whereas coating ourselves with PEI or PDL and laminin generally caused neuron clumping or constant axon collapse.

Our work also emphasized the importance of having iPSCs from multiple individuals and multiple clones paired with appropriate controls like tau knockdown and knockout. We acknowledge that there are limitations to our studies. Our neurons under the conditions we used only express a single isoform of tau, the fetal isoform 0N3R. Understanding how different tau isoforms are regulated and how they contribute tau function in health and disease is an open question. Our findings would also be strengthened by further work in a complementary model system or in human brain tissue. There was substantial overlap between our findings and a recent paper using *MAPT* V337M neurons in an organoid model [9]. We anticipate that data from

human patients will be forthcoming and will further support our discovery. We aim to validate our findings in animal models and human tissue. Recent work demonstrated that in cortical neurons, *MAP1B* phosphorylation by *GSK3B* promotes axon branching by modifying tubulin tyrosination [35]. Unphosphorylated *MAP1B* restricts axon branching *in vivo*. In our model, *MAP1B* is dephosphorylated despite rampant axon branching. This supports the model that *MAPT V337M* is promoting axon branching while the neurons are unsuccessfully attempting to downregulate axon branching. The other transcriptomic and proteomic signatures point to multiple layers of regulation around axonogenesis are likely also in response to the aberrant axon branching induced by *MAPT V337M*. We predict that tau knockout mice and tauopathy mice will have robust transcriptomic signatures reflecting changes in gene expression of axonogenesis genes in response to tau loss of function.

Additionally, the convergence between *MYO1B* knockdown causing axon branching and tau loss of function causing axon branching is perplexing given that V337M tau likely binds more to *MYO1B* than WT tau [24]. Further mechanistic work is needed to address how exactly V337M tau and *MYO1B* cause axon branching in our neurons. One attractive hypothesis is that V337M tau causes increased polymerization of tyrosinated tubulin into the peripheral zone of growth cones, which is enriched for *MYO1B*. If true, it would mean that *MYO1B* interacting with V337M tau is a consequence rather than directly responsible for changes in axon branching.

The normal function of tau is unclear and has been debated for many years. This is in large part due to the many conflicting studies, both in a physiological and pathogenic context. Given the earlier results in showing tau's importance for axonogenesis, it was expected that knocking tau

out in mice would be lethal and that tau would be essential for neurodevelopment. Early mouse studies showed that tau knockout was surprisingly well tolerated [41]. There were no obvious defects in polarization or gross morphology, but microtubules in small caliber axons were destabilized. MAP1A was upregulated in tau knockout mice, suggesting that the mice were compensating for tau loss. This could explain the difference in phenotypes as compared to the acute depletion of tau with ASOs. Knocking out tau and another microtubule associated protein, like *MAP1B* lead to much more severe phenotypes than either knockout individually [42]. Dawson et al. disputed the findings of Harada et al. due to poor WT data [43]. In their work, found that indeed tau knockout did cause a delay in neurite outgrowth and axonogenesis.

More recent work has identified that tau plays an important role in regulating microtubule dynamics in growth cones [44]. Biswas and Kalil showed that tau knockout neurons had altered microtubule dynamics in growth cones, resulting in a change in overall growth cone morphology. Microtubules were less bundled, and microtubule polymerization directionality as measured by EB3 was more dispersed in tau knockout neurons. There also was a reduction in tyrosinated tubulin projecting into the filopodia of the peripheral domain. Another paper showed that tau knockout increased Fyn mobility in dendrites and lowered Fyn localization in dendrites and spines [45]. Intriguingly, expressing P301L tau had the opposite effect and anchored or trapped Fyn in dendritic spines.

Many motor and behavioral phenotypes have been observed in tau knockout mice. Tau knockout mice or mice with acute tau reduction with antisense oligonucleotides have consistently shown resistance to seizures [21, 46-49]. Another consistent theme is that there are often behavioral and

learning changes in tau knockout mice, including hyperactivity, fear conditioning, and memory [50-55]. There is more controversy over the effect of tau knockout on motor function. Some groups report motor deficits in tau knockout mice [50, 56, 57], while others claim there are no significant changes in tau knockout mice to motor function [46, 47, 55]. One group showed that tau is essential for long term depression in the hippocampus [58], while another showed that tau knockout only perturbs long term potentiation [55]. Tau phosphorylation has also been shown to be required for long term depression [59].

The loss of function phenotypes coincide with the onset of tau expression and axon extension, and the toxic gain of function phenotypes coincide with synaptogenesis and the onset of neuronal activity. These dual pathways provide further insight into how the *MAPT* V337M mutation dysregulate neurons in human disease. Tau loss of function would precede human disease onset by many decades, occurring during development and continuing through adulthood via perturbed synaptic plasticity. A study showed that mice with the *MAPT* P301L mutation show early cognitive changes before tau pathology is detectable [60]. A Parkinson's disease GWAS study found that *MAPT* was a significant risk locus for Parkinson's disease that is uncoupled from the age of onset [61]. Ye and colleagues proposed that tau may drive changes during development or early in life that then increase risk for Parkinson's disease decades later [62]. Two studies have also identified cognitive differences between *MAPT* carriers and non-carrier siblings decades before expected disease onset [63, 64].

Taking all these data together, despite the noise and discrepancies, tau clearly has a role in axonogenesis during development and in synaptic plasticity throughout life. Given the strong

link with neuronal excitability and neurodegenerative diseases like Alzheimer's and Frontotemporal Dementia, a model of a vicious cycle where tau and neuronal excitability feedback on each other either from a tau-first insult (FTD) or neuronal excitability insult (AD) could provide a unifying mechanism explaining tauopathy pathogenesis.

MATERIALS AND METHODS:

Sample preparation and data acquisition

Human iPSC culture and neuronal differentiation (Adapted from Tian et al. 2021)

Human iPSCs from the WTC11 background were cultured in StemFlex Medium (GIBCO/Thermo Fisher Scientific; Cat. No. A3349401). Human iPSCs from the GIH6C1 background were cultured in mTeSR Plus medium (StemCell Technologies; Cat. No. 100-0276). iPSCs were grown in plates or dishes coated with Growth Factor Reduced, Phenol Red-Free, LDEV-Free Matrigel Basement Membrane Matrix (Corning; Cat. No. 356231) diluted 1:100 in Knockout DMEM (GIBCO/Thermo Fisher Scientific; Cat. No. 10829-018). StemFlex Medium was replaced daily. When cells reached 80-90% confluency, cells were dissociated with StemPro Accutase Cell Dissociation Reagent (GIBCO/Thermo Fisher Scientific; Cat. No. A11105-01) at 37°C for 5 min, centrifuged at 200 g for 5 min, resuspended in StemFlex Medium supplemented with 10 nM Y-27632 dihydrochloride ROCK inhibitor (Tocris; Cat. No. 125410) and placed onto Matrigel-coated plates or dishes. Studies at UCSF with human iPSCs were approved by the Human Gamete, Embryo, and Stem Cell Research (GESCR) Committee.

For individual gene knockdown in CRISPRi iPSCs, sgRNAs were introduced into iPSCs via lentiviral delivery. Cells were selected by 1 µg/ml puromycin for 2-4 days and recovered for 2-4 days. Phenotypes were evaluated 5-7 days after infection.

The WTC11 CRISPRi iPSC lines were previously engineered to express mNGN2 under a doxycycline-inducible system in the AAVS1 safe harbor locus. The GIH6C1 iPSC lines were engineered in this work to express mNGN2 under a doxycycline-inducible promoter in the AAVS1 safe harbor locus. For their neuronal differentiation, we followed our previously described protocol [25]. Briefly, iPSCs were pre-differentiated in matrigel-coated plates or dishes in N2 Pre-Differentiation Medium containing the following: Knockout DMEM/F12 (GIBCO/Thermo Fisher Scientific; Cat. No. 12660-012) as the base, 1X MEM Non-Essential Amino Acids (GIBCO/Thermo Fisher Scientific; Cat. No. 17502-048), 10 ng/mL NT-3 (PeproTech; Cat. No. 450-03), 10 ng/mL BDNF (PeproTech; Cat. No. 450-02), 1 µg/mL Mouse Laminin (Thermo Fisher Scientific; Cat. No. 23017-015), 10 nM ROCK inhibitor and 2 µg/mL doxycycline to induce the expression of mNGN2. After three days, or Day 0, pre-differentiated cells were dissociated with accutase and plated into BioCoat Poly-D-Lysine-coated plates or dishes (Corning; assorted Cat. No.) in Classic N2 neuronal medium or BrainPhys Neuronal Medium. Classic N2 neuronal medium contained the following: half DMEM/F12 (GIBCO/Thermo Fisher Scientific; Cat. No. 11320-033) and half Neurobasal-A (GIBCO/Thermo Fisher Scientific; Cat. No. 10888-022) as the base, 1X MEM Non-Essential Amino Acids, 0.5X GlutaMAX Supplement (GIBCO/Thermo Fisher Scientific; Cat. No. 35050-061), 0.5X N2 Supplement, 0.5X B27 Supplement (GIBCO/Thermo Fisher Scientific; Cat. No. 17504-044), 10 ng/mL NT-3, 10 ng/mL BDNF and 1 µg/mL Mouse Laminin. BrainPhys Neuronal Medium was

comprised of the following: BrainPhys Neuronal Medium (StemCell Technologies; Cat. No. 05791) as the base, 0.5x N2 Supplement, 0.5X B27 Supplement, 10 ng/mL NT-3, 10ng/mL BDNF, and 1 µg/mL Mouse Laminin. Neuronal medium was fully changed on day 3 post differentiation and then half-replaced on day 7 and weekly thereafter.

Molecular Cloning

pGM22 was cloned by introducing the V337M mutation to 0N3R tau by site-directed mutagenesis. The backbone containing CAG-GFP-0N3Rtau^{WT} (pAJS1149, a gift from Avi Samelson) and insert were digested with AgeI and XhoI.

GIH6C1 iPSC cell line generation

GIH6C1 and GIH6C1Δ1E11 were given to us by NeuraCell [REF]. iPSCs were transfected with pC13N-dCas9-BFP-KRAB and TALENS targeting the human CLYBL intragenic safe harbor locus (between exons 2 and 3) (pZT-C13-R1 and pZT-C13-L1, Addgene #62196, #62197) using DNA In-Stem (VitaScientific). At the same time, the iPSCs were also transfected with E42 pUCM-TO-mNGN2 and TALENS targeting the human AAVS1 intragenic safe harbor locus (PLASMID IDs). After two weeks, BFP-positive iPSCs (CRISPRi⁺/mNGN2⁻), mCherry-positive iPSCs (CRISPRi⁻/mNGN2⁺) and BFP/mCherry-positive iPSCs (CRISPRi⁺/mNGN2⁺) were isolated via FACS sorting. Cells were plated sparsely in a 10 cm dish (5,000-10,000 per dish) and allowed to grow up until they formed large colonies. Homogenous BFP⁺/mCherry⁺ colonies were picked with a pipette tip and placed into a 24 well plate for expansion and characterization. Cre mRNA was then transfected into the iPSCs to remove the selection marker and mCherry. Cells were sorted for mCherry negativity, and then mCherry negative colonies were picked and genotyped.

Immunofluorescence

Neurons were washed in PBS, fixed with 4% PFA, washed 3x in PBS and blocked with TBS⁴⁺. The neurons were then stained overnight at 4°C with primary antibody diluted in TBS⁴⁺. The next day, the neurons were washed 3x with TBS and stained with secondary antibody diluted in TBS⁴⁺ for one hour at room temperature. The secondary antibody was washed 3x with TBS and then the neurons were maintained in TBS.

Drug treatments

Oligomycin and Rotenone were diluted in anti-oxidant free media as described previously [28]. Neuronal media was fully replaced with anti-oxidant free media with vehicle (DMSO) or drug treatment. DMSO concentrations were kept constant across all conditions, and the final concentration of DMSO was always less than 0.1%.

Western blots

Neurons were washed 3 times with ice-cold PBS. Ice-cold RIPA with protease and phosphatase inhibitors was added to cells. Lysates were incubated on ice for 2 minutes and then scraped down. Lysates were centrifuged at 12500xg for 10 minutes at 4 °C. The supernatants were collected, and the concentrations were measured with the BCA assay (Thermo Fisher Scientific; Cat No. 23225). 10-20 µg protein were loaded onto 4-12% Bis-Tris polyacrylamide gel (Thermo Fisher Scientific; Cat No. NP0336BOX) Nitrocellulose (BioRad, Cat. No. 1620146) or PVDF membranes were used to transfer the protein in a BioRad Transblot for 11 minutes at 25 V, 25 A. Membranes were then blocked for 1 hour with Licor Intercept blocking buffer (Licor, Cat. No.

927-60001) at room temperature. Primary antibody was added in Licor Intercept block overnight at 4 °C. Blots were washed 3 times for 5 minutes with TBST at room temperature. Secondary antibodies were added in Licor Intercept block for 1 hour at room temperature. Blots were washed 3 times for 5 minutes with TBST at room temperature and imaged on a Licor Odyssey. Immunoblots were quantified by intensity using ImageStudio (Licor).

Bulk RNA sequencing sample preparation

RNA was harvested from day 7, day 14 and day 28 post differentiation neurons using a Zymo microprep kit (Zymo Research, Cat No. R2062). The library was prepared by first depleting ribosomal RNA (New England BioLabs, Cat No. E7405L). cDNA synthesis was then performed on all remaining RNAs (New England BioLabs, Cat. No. E7765S). Sequencing was performed at the Chan Zuckerberg Biohub and the UCSF Center for Advanced Technology.

ATAC-seq sample preparation

Cells were treated with Tn5 transposase to tag and cleave open chromatin with PCR adapters. Tagged sequences were purified, amplified and sequenced by high throughput sequencing.

Proteomics sample preparation

Briefly, neurons were scraped off 15 cm dishes at day 7 of differentiation and flash frozen in liquid nitrogen. Cell pellet was lysed by adding 1 ml of 6 M GnHCl, 100mM Tris pH 8 and boiling at 95 C for 5 minutes two times with 5 min rest in between. DNA was sheared three times via probe sonication at 20% amplitude for 10 s., followed by 10 s of rest. Following sonication, samples were allowed to solubilize on ice for 20 mins before clearing cell debris by

centrifugation at 16,000 x g for 10 mins and determining protein concentration was using Protein Thermo Scientific 660 assay. Enough lysate for 1 mg of protein was aliquoted and Tris 2-carboxyethyl phosphine (TCEP) and chloroacetamide (CAA) were added to each sample to a final concentration of 40 mM and 10 mM respectively, before incubating for 10 min at 45 C with shaking. Guanidine was then diluted at least 1:5 with 100 mM Tris pH 8. Trypsin and LysC (Promega) were added at a 1:100 (enzyme:protein w:w) ratio (total protease:protein ratio of 1:50) and digested overnight at 37°C with shaking. Following digestion, 10% trifluoroacetic acid (TFA) was added to each sample to a final pH ~2. Samples were desalted under vacuum using Sep Pak tC18 cartridges (Waters). Each cartridge was activated with 1 mL 80% acetonitrile (ACN)/0.1% TFA, then equilibrated with 3 × 1 mL of 0.1% TFA. Cartridges were then washed with 4 × 1 mL of 0.1% TFA, and samples were eluted with 0.8 mL 50% ACN/0.25% formic acid (FA). 20 µg of each sample was kept for protein abundance measurements, and the remainder was used for phosphopeptide enrichment. Samples were dried by vacuum centrifugation.

Phosphopeptide enrichment

For phosphopeptide enrichment of samples for phosphoproteomics, IMAC beads (Fe-IMAC from Cube Biotech) were prepared by washing 3x with washing buffer (0.1% TFA, 80% ACN). Dry, digested peptide samples were resuspended in washing buffer and incubated for 15 mins at 37 C with shaking. Peptides were enriched for phosphorylated peptides using a King Fisher Flex (KFF). A more detailed KFF protocol can be provided. Briefly, after resuspension peptides were mixed with beads and bound peptides were washed three times with wash buffer before being eluted from beads using 50% ACN, 2.5 % NH₄OH solution. Enriched phosphorylated peptide samples were acidified using 75% ACN, 10% FA (at a ratio of 5:3 elution buffer:acid buffer), and filtered by centrifugation through NEST tips.

Mass spectrometry data acquisition

Digested samples were analyzed on an Orbitrap Exploris 480 mass spectrometry system (Thermo Fisher Scientific) equipped with either an Easy nLC 1200 or Neo Vanquish ultra-high pressure liquid chromatography system (Thermo Fisher Scientific) interfaced via a Nanospray Flex source. Separation was performed using a 15 cm long PepSep column with a 150 μm inner diameter packed with 1.5 μm Reprosil C18 particles. Mobile phase A consisted of 0.1% FA, and mobile phase B consisted of 0.1% FA/80% ACN. Abundance samples were separated by an organic gradient from 4% to 30% mobile phase B over 62 minutes followed by an increase to 45% B over 10 minutes, then held at 90% B for 8 minutes at a flow rate of 600 nL/minute. Phosphoproteomics samples were separated by an organic gradient from 2% to 25% mobile phase B over 62 minutes followed by an increase to 40% B over 10 minutes, then held at 95% B for 8 minutes at a flow rate of 600 nL/minute. To expand the spectral library, two samples from each set of biological replicates was acquired in a data dependent manner. Data dependent analysis (DDA) was performed by acquiring a full scan over a m/z range of 350-1100 in the Orbitrap at 60,000 resolving power (@200 m/z) with a normalized AGC target of 300%, an RF lens setting of 40%, and a maximum ion injection time of "Auto". Dynamic exclusion was set to 45 seconds, with a 10 ppm exclusion width setting. Peptides with charge states 2-6 were selected for MS/MS interrogation using higher energy collisional dissociation (HCD), with 20 MS/MS scans per cycle. MS/MS scans were analyzed in the Orbitrap using isolation width of 1.6 m/z , normalized HCD collision energy of 30%, normalized AGC of 200% at a resolving power of 15,000 with a 22 ms maximum ion injection time. Similar settings were used for data dependent analysis of phosphopeptide-enriched and abundance samples. Data-independent analysis (DIA)

was performed on all samples. An MS scan at 60,000 resolving power over a scan range of 350-1100 m/z, a normalized AGC target of 300%, an RF lens setting of 40%, and the maximum injection time set to “Auto”, followed by DIA scans using 20 m/z isolation windows over 350-1100 m/z with a 2 m/z overlap at a normalized HCD collision energy of 30%.

Survival Timecourse Imaging

20,000 neurons were plated in Black Corning Biocoat clear bottom 96-well plates. Neurons were imaged daily for two weeks. Neurons expressing nuclear localized BFP lose their BFP signal when they undergo cell death, so the number of live neurons in a well was approximated over time by counting the number BFP nuclei CellProfiler and subtracting the number of nuclei that are BFP positive and Caspase-3/7 or Topro3 positive.

Longitudinal Neurite Imaging

20,000 neurons were plated in Black Corning Biocoat clear bottom 96-well plates. The background cells were unlabeled *MAPT* WT neurons without any markers or sgRNAs. Neurons labeled with LCK-mNeonGreen were plated at a density of 2-30 cells per well and were imaged every other day from day 1 to day 11 of differentiation. Images were collected on an InCell6000 using a 10x objective. Thirty six fields per well with 15% overlap were used to image the entire well.

Antibodies used in this study

MYO1B (abcam, ab194356)

cJun (CST, #9165)

p-cJun (CST, #91952)

GFP (CST, #2956)

HT7 (ThermoFisher Scientific, MN1000)

Tau13 (Santa Cruz Biotechnology, sc-21796)

OXPHOS Cocktail (abcam, ab110411)

TOM20 (CST, #42406)

SDHA (Santa Cruz Biotechnology, sc-166947)

GAPDH (Santa Cruz Biotechnology, sc-47724)

β -Actin (CST, #4967)

Data Analysis

RNA-seq

Sequencing data was aligned to the human reference genome hg38. Rbowtie2 was used to align and count the number of transcripts from aligned reads. Differentially expressed genes were determined using DEseq2.

ATAC-seq

Sequencing data was aligned to the human reference genome hg38 using Rbowtie2. Peak calling was performed with MACS2. Differential ATACseq was performed using DEseq2, and motif analysis was performed with the motifDB and motifmatchr packages. Differential motif analysis was performed with the chromVar package.

Gene set enrichment analysis

Enrichr was used to perform gene set enrichment analysis on RNA-seq, proteomics and phosphoproteomics datasets [65].

Proteomics and Phosphoproteomics

Raw files were searched using the directDIA+ feature in Spectronaut, with DDA files provided as supplementary search files against a full human proteome from Uniprot (reviewed entries only, isoforms included). Phosphosites were extracted from the PTMsites output table from Spectronaut, and collapsed using the Tukey's median polish functionality of MSstats in R.

Longitudinal image analysis

Brightfield images were stitched first using FIJI's Grid/Collection stitch plugin [66]. The configuration files were then formatted to be compatible with the MIST stitching plugin, which allows input configuration files to be applied to other images [67]. The LCK-mNeonGreen images were then stitched using the brightfield coordinates with MIST. Images were blinded with a simple python script written by a colleague that changed the names of the images to another number greater than what is found in a 96 well plate (ex: B02 becomes B68). Blinded images were then manually traced and measured in FIJI. The longest primary neurite was considered to be the axon. Branches from that axon were considered to be axon branches. Additional neurites extending from the soma were considered secondary neurites. The measurement files were then unblinded by a complementary python script. The unblinded data was imported into R, processed, and then plotted in Prism for visualization. Statistical analysis

was performed in Prism. Two-Way ANOVA with Dunnett's multiple comparison test was carried out on longitudinal data. One-way ANOVA with Dunnett's multiple comparison test was performed on single timepoint data.

REFERENCES

1. Alzheimer, A., *Über eigenartige Erkrankung der Hirnrinde*. All Z Psychiatr, 1907. **64**: p. 146-148.
2. Malpetti, M., R. Joie, and G.D. Rabinovici, *Tau Beats Amyloid in Predicting Brain Atrophy in Alzheimer Disease: Implications for Prognosis and Clinical Trials*. J Nucl Med, 2022. **63**(6): p. 830-832.
3. Wu, L., et al., *Early-onset familial Alzheimer's disease (EOFAD)*. Can J Neurol Sci, 2012. **39**(4): p. 436-45.
4. Wang, Y. and E. Mandelkow, *Tau in physiology and pathology*. Nat Rev Neurosci, 2016. **17**(1): p. 5-21.
5. Silva, M.C., et al., *Human iPSC-Derived Neuronal Model of Tau-A152T Frontotemporal Dementia Reveals Tau-Mediated Mechanisms of Neuronal Vulnerability*. Stem Cell Reports, 2016. **7**(3): p. 325-340.
6. Ash, P.E.A., et al., *TIA1 potentiates tau phase separation and promotes generation of toxic oligomeric tau*. Proc Natl Acad Sci U S A, 2021. **118**(9).
7. Jiang, L., et al., *Interaction of tau with HNRNPA2B1 and N(6)-methyladenosine RNA mediates the progression of tauopathy*. Mol Cell, 2021. **81**(20): p. 4209-4227 e12.
8. Lester, E., et al., *Tau aggregates are RNA-protein assemblies that mislocalize multiple nuclear speckle components*. Neuron, 2021. **109**(10): p. 1675-1691 e9.
9. Bowles, K.R., et al., *ELAVL4, splicing, and glutamatergic dysfunction precede neuron loss in MAPT mutation cerebral organoids*. Cell, 2021. **184**(17): p. 4547-4563 e17.

10. Dickson, J.R., M.P. Frosch, and B.T. Hyman, *Altered localization of nucleoporin 98 in primary tauopathies*. *Brain Commun*, 2023. **5**(1): p. fcac334.
11. Frost, B., F.H. Bardai, and M.B. Feany, *Lamin Dysfunction Mediates Neurodegeneration in Tauopathies*. *Curr Biol*, 2016. **26**(1): p. 129-36.
12. Paonessa, F., et al., *Microtubules Deform the Nuclear Membrane and Disrupt Nucleocytoplasmic Transport in Tau-Mediated Frontotemporal Dementia*. *Cell Rep*, 2019. **26**(3): p. 582-593 e5.
13. Stamer, K., et al., *Tau blocks traffic of organelles, neurofilaments, and APP vesicles in neurons and enhances oxidative stress*. *J Cell Biol*, 2002. **156**(6): p. 1051-63.
14. Vossel, K.A., et al., *Tau reduction prevents Abeta-induced axonal transport deficits by blocking activation of GSK3beta*. *J Cell Biol*, 2015. **209**(3): p. 419-33.
15. DuBoff, B., J. Gotz, and M.B. Feany, *Tau promotes neurodegeneration via DRP1 mislocalization in vivo*. *Neuron*, 2012. **75**(4): p. 618-32.
16. Caballero, B., et al., *Acetylated tau inhibits chaperone-mediated autophagy and promotes tau pathology propagation in mice*. *Nat Commun*, 2021. **12**(1): p. 2238.
17. Sohn, P.D., et al., *Pathogenic Tau Impairs Axon Initial Segment Plasticity and Excitability Homeostasis*. *Neuron*, 2019. **104**(3): p. 458-470 e5.
18. Chang, C.W., et al., *Tau reduction affects excitatory and inhibitory neurons differently, reduces excitation/inhibition ratios, and counteracts network hypersynchrony*. *Cell Rep*, 2021. **37**(3): p. 109855.
19. Ittner, L.M., et al., *Dendritic function of tau mediates amyloid-beta toxicity in Alzheimer's disease mouse models*. *Cell*, 2010. **142**(3): p. 387-97.

20. Miyamoto, T., et al., *Phosphorylation of tau at Y18, but not tau-fyn binding, is required for tau to modulate NMDA receptor-dependent excitotoxicity in primary neuronal culture*. Mol Neurodegener, 2017. **12**(1): p. 41.
21. Roberson, E.D., et al., *Reducing endogenous tau ameliorates amyloid beta-induced deficits in an Alzheimer's disease mouse model*. Science, 2007. **316**(5825): p. 750-4.
22. Chang, C.W., E. Shao, and L. Mucke, *Tau: Enabler of diverse brain disorders and target of rapidly evolving therapeutic strategies*. Science, 2021. **371**(6532).
23. Karch, C.M., et al., *A Comprehensive Resource for Induced Pluripotent Stem Cells from Patients with Primary Tauopathies*. Stem Cell Reports, 2019. **13**(5): p. 939-955.
24. Tracy, T.E., et al., *Tau interactome maps synaptic and mitochondrial processes associated with neurodegeneration*. Cell, 2022. **185**(4): p. 712-728 e14.
25. Tian, R., et al., *CRISPR Interference-Based Platform for Multimodal Genetic Screens in Human iPSC-Derived Neurons*. Neuron, 2019. **104**(2): p. 239-255 e12.
26. Paoletti, P., C. Bellone, and Q. Zhou, *NMDA receptor subunit diversity: impact on receptor properties, synaptic plasticity and disease*. Nat Rev Neurosci, 2013. **14**(6): p. 383-400.
27. Kolodkin, A.L. and M. Tessier-Lavigne, *Mechanisms and molecules of neuronal wiring: a primer*. Cold Spring Harb Perspect Biol, 2011. **3**(6).
28. Tian, R., et al., *Genome-wide CRISPRi/a screens in human neurons link lysosomal failure to ferroptosis*. Nat Neurosci, 2021. **24**(7): p. 1020-1034.
29. Schmidt, E.F. and S.M. Strittmatter, *The CRMP family of proteins and their role in Sema3A signaling*. Adv Exp Med Biol, 2007. **600**: p. 1-11.

30. Cuadrado, A. and A.R. Nebreda, *Mechanisms and functions of p38 MAPK signalling*. *Biochem J*, 2010. **429**(3): p. 403-17.
31. Falcicchia, C., et al., *Involvement of p38 MAPK in Synaptic Function and Dysfunction*. *Int J Mol Sci*, 2020. **21**(16).
32. UniProt, C., *UniProt: the Universal Protein Knowledgebase in 2023*. *Nucleic Acids Res*, 2023. **51**(D1): p. D523-D531.
33. Trivedi, N., et al., *Glycogen synthase kinase-3beta phosphorylation of MAP1B at Ser1260 and Thr1265 is spatially restricted to growing axons*. *J Cell Sci*, 2005. **118**(Pt 5): p. 993-1005.
34. Barnat, M., et al., *The GSK3-MAP1B pathway controls neurite branching and microtubule dynamics*. *Mol Cell Neurosci*, 2016. **72**: p. 9-21.
35. Ziak, J., et al., *MAP1B Regulates Cortical Neuron Interstitial Axon Branching Through the Tubulin Tyrosination Cycle*. *bioRxiv*, 2023: p. 2023.10.02.560024.
36. Iuliano, O., et al., *Myosin Ib promotes axon formation by regulating actin wave propagation and growth cone dynamics*. *J Cell Biol*, 2018. **217**(6): p. 2033-2046.
37. Sun, N., et al., *Measuring In Vivo Mitophagy*. *Mol Cell*, 2015. **60**(4): p. 685-96.
38. Caceres, A., S. Potrebic, and K.S. Kosik, *The effect of tau antisense oligonucleotides on neurite formation of cultured cerebellar macroneurons*. *J Neurosci*, 1991. **11**(6): p. 1515-23.
39. Caceres, A. and K.S. Kosik, *Inhibition of neurite polarity by tau antisense oligonucleotides in primary cerebellar neurons*. *Nature*, 1990. **343**(6257): p. 461-3.
40. Morris, S.L. and S.T. Brady, *Tau phosphorylation and PAD exposure in regulation of axonal growth*. *Front Cell Dev Biol*, 2022. **10**: p. 1023418.

41. Harada, A., et al., *Altered microtubule organization in small-calibre axons of mice lacking tau protein*. Nature, 1994. **369**(6480): p. 488-91.
42. Takei, Y., et al., *Defects in axonal elongation and neuronal migration in mice with disrupted tau and map1b genes*. J Cell Biol, 2000. **150**(5): p. 989-1000.
43. Dawson, H.N., et al., *Inhibition of neuronal maturation in primary hippocampal neurons from tau deficient mice*. J Cell Sci, 2001. **114**(Pt 6): p. 1179-87.
44. Biswas, S. and K. Kalil, *The Microtubule-Associated Protein Tau Mediates the Organization of Microtubules and Their Dynamic Exploration of Actin-Rich Lamellipodia and Filopodia of Cortical Growth Cones*. J Neurosci, 2018. **38**(2): p. 291-307.
45. Padmanabhan, P., et al., *Frontotemporal dementia mutant Tau promotes aberrant Fyn nanoclustering in hippocampal dendritic spines*. Elife, 2019. **8**.
46. Tan, D.C.S., et al., *Generation of a New Tau Knockout (tauDeltaex1) Line Using CRISPR/Cas9 Genome Editing in Mice*. J Alzheimers Dis, 2018. **62**(2): p. 571-578.
47. Li, Z., et al., *Seizure resistance without parkinsonism in aged mice after tau reduction*. Neurobiol Aging, 2014. **35**(11): p. 2617-2624.
48. Gheyara, A.L., et al., *Tau reduction prevents disease in a mouse model of Dravet syndrome*. Ann Neurol, 2014. **76**(3): p. 443-56.
49. DeVos, S.L., et al., *Antisense reduction of tau in adult mice protects against seizures*. J Neurosci, 2013. **33**(31): p. 12887-97.
50. Velazquez, R., et al., *Acute tau knockdown in the hippocampus of adult mice causes learning and memory deficits*. Aging Cell, 2018. **17**(4): p. e12775.

51. Oberrauch, S., et al., *Reward motivation and cognitive flexibility in tau null-mutation mice*. *Neurobiol Aging*, 2021. **100**: p. 106-117.
52. Ikegami, S., A. Harada, and N. Hirokawa, *Muscle weakness, hyperactivity, and impairment in fear conditioning in tau-deficient mice*. *Neurosci Lett*, 2000. **279**(3): p. 129-32.
53. Goncalves, R.A., et al., *Behavioral Abnormalities in Knockout and Humanized Tau Mice*. *Front Endocrinol (Lausanne)*, 2020. **11**: p. 124.
54. Cheng, J.S., et al., *Tau reduction diminishes spatial learning and memory deficits after mild repetitive traumatic brain injury in mice*. *PLoS One*, 2014. **9**(12): p. e115765.
55. Ahmed, T., et al., *Cognition and hippocampal synaptic plasticity in mice with a homozygous tau deletion*. *Neurobiol Aging*, 2014. **35**(11): p. 2474-2478.
56. Morris, M., et al., *Age-appropriate cognition and subtle dopamine-independent motor deficits in aged tau knockout mice*. *Neurobiol Aging*, 2013. **34**(6): p. 1523-9.
57. Lei, P., et al., *Motor and cognitive deficits in aged tau knockout mice in two background strains*. *Mol Neurodegener*, 2014. **9**: p. 29.
58. Kimura, T., et al., *Microtubule-associated protein tau is essential for long-term depression in the hippocampus*. *Philos Trans R Soc Lond B Biol Sci*, 2014. **369**(1633): p. 20130144.
59. Regan, P., et al., *Tau phosphorylation at serine 396 residue is required for hippocampal LTD*. *J Neurosci*, 2015. **35**(12): p. 4804-12.
60. Boekhoorn, K., et al., *Improved long-term potentiation and memory in young tau-P301L transgenic mice before onset of hyperphosphorylation and tauopathy*. *J Neurosci*, 2006. **26**(13): p. 3514-23.

61. Blauwendraat, C., et al., *Parkinson's disease age at onset genome-wide association study: Defining heritability, genetic loci, and alpha-synuclein mechanisms*. *Mov Disord*, 2019. **34**(6): p. 866-875.
62. Ye, H., et al., *Genetics and Pathogenesis of Parkinson's Syndrome*. *Annu Rev Pathol*, 2023. **18**: p. 95-121.
63. Finger, E., et al., *Neurodevelopmental effects of genetic frontotemporal dementia in young adult mutation carriers*. *Brain*, 2023. **146**(5): p. 2120-2131.
64. Geschwind, D.H., et al., *Dementia and neurodevelopmental predisposition: cognitive dysfunction in presymptomatic subjects precedes dementia by decades in frontotemporal dementia*. *Ann Neurol*, 2001. **50**(6): p. 741-6.
65. Chen, E.Y., et al., *Enrichr: interactive and collaborative HTML5 gene list enrichment analysis tool*. *BMC Bioinformatics*, 2013. **14**: p. 128.
66. Preibisch, S., S. Saalfeld, and P. Tomancak, *Globally optimal stitching of tiled 3D microscopic image acquisitions*. *Bioinformatics*, 2009. **25**(11): p. 1463-5.
67. Chalfoun, J., et al., *MIST: Accurate and Scalable Microscopy Image Stitching Tool with Stage Modeling and Error Minimization*. *Sci Rep*, 2017. **7**(1): p. 4988.

Publishing Agreement

It is the policy of the University to encourage open access and broad distribution of all theses, dissertations, and manuscripts. The Graduate Division will facilitate the distribution of UCSF theses, dissertations, and manuscripts to the UCSF Library for open access and distribution. UCSF will make such theses, dissertations, and manuscripts accessible to the public and will take reasonable steps to preserve these works in perpetuity.

I hereby grant the non-exclusive, perpetual right to The Regents of the University of California to reproduce, publicly display, distribute, preserve, and publish copies of my thesis, dissertation, or manuscript in any form or media, now existing or later derived, including access online for teaching, research, and public service purposes.

DocuSigned by:
Greg Mohl
602338E290D2431... _____
Author Signature

10/18/2023
Date